Sensor and Simulation Notes

Note 283

28 March 1983

Idealized Electric- and Magnetic-Field Sensors
Based on Spherical Sheet Impedances

Carl E. Baum
Air Force Weapons Laboratory

Abstract

This note considers the response of electric- and magnetic-field sensors in terms of spherical modal expansions to identify the electric- and magnetic-dipole terms which are associated with the ideal angular response to an incident plane wave. Considering an idealized spherical resistive sheet sensor, the dipole surface current densities are computed and bandwidth and figure of merit determined to optimize the choice of R_s.

For practical sensors the response in general includes various multipole terms besides the desired dipole terms. Expanding the response in terms of spherical harmonics allows one to identify the dipole term and from this gives one a definition of upper frequency response. In addition a norm over the unit sphere of the difference between the actual response and the ideal response gives another way to define upper frequency response.

An example of a magnetic-sensor design which approximates the resistive-sheet sphere is also considered.

Acknowledgement

I.   Introduction

For some time now consideration has been given to the design of optimum sensors for the time derivative of electromagnetic field components in free-space conditions. Various sensors for components of $\partial \vec{B}/\partial t$ and $\partial \vec{D}/\partial t$ have been constructed for EMP and lightning applications [7,8,9]. The response of these sensors is fundamentally limited by transit times of the electromagnetic wave across the sensor structure [6]. Besides accuracy considerations, an optimum sensor design can be defined as one that maximizes bandwidth (related to this transit-time limitation) for a given sensitivity.

A previous note has considered some fundamental aspects of this trade-off between sensitivity and bandwidth and has defined appropriate dimensionless figures of merit for both electric and magnetic types of derivative sensors [6]. The reader should consult this previous paper for various results not repeated here. In the present paper the sensor is assumed to be in a free-space configuration so that the assumed incident plane wave can arrive from any direction (4π steradians). These results can be related to sensors mounted on ground planes using the expressions in [6].

   a.   Basic expressions for figure of merit

Based on voltage and current, respectively, the dimensionless figures of merit are

$$\Lambda^{(V)} = \left| \frac{\tilde{V}_{ideal}(j\omega_c)}{\tilde{E}_{ref}(j\omega_c)} \right| \frac{1}{\ell_c} \tag{1.1}$$

$$\Lambda^{(I)} = \left| \frac{\tilde{I}_{ideal}(j\omega_c)}{\tilde{H}_{ref}(j\omega_c)} \right| \frac{1}{\ell_c}$$

where

$$\ell_c = ct_c = \frac{c}{\omega_c}$$

$\omega_c \equiv$ upper frequency response (defined in some appropriate way)

$t_c \equiv$ some characteristic rise time

$\ell_c \equiv$ an associated characteristic length

$$\tag{1.2}$$

The ideal voltages and currents are based on the low-frequency (quasi-static) form of the sensor response. For electric-dipole sensors we have

$$\tilde{V}_{ideal}(s) = Z_c \tilde{I}_{ideal}(s) = -sZ_c \vec{A}_{e_{eq}} \cdot \tilde{\vec{D}}_{inc}(s)$$

(1.3)

$$\vec{A}_{e_{eq}} \equiv \text{equivalent area (quasi-static, independent of s)}$$

$$\vec{D}_{inc}(t) \equiv \text{incident electric flux density evaluated at "center"}$$
of sensor (typically coordinate origin)

and for magnetic-dipole sensors we have

$$\tilde{V}_{ideal}(s) = Z_c \tilde{I}_{ideal}(s) = s\vec{A}_{h_{eq}} \cdot \tilde{\vec{B}}_{inc}(s)$$

(1.4)

$$\vec{A}_{h_{eq}} \equiv \text{equivalent area (quasi-static, independent of s)}$$

$$\vec{B}_{inc}(t) \equiv \text{incident magnetic flux density evaluated at "center"}$$
of sensor (typically coordinate origin)

with

$t \equiv$ time

$s \equiv$ complex frequency or Laplace-transform variable ($= j\omega$ for frequency-domain analysis)

(1.5)

$\sim \equiv$ designator of Laplace-transformed (two-sided) quantity

$Z_c \equiv$ impedance (assumed a constant resistance) driven by sensor

Some other physical parameters are

$$c = \frac{1}{\sqrt{\mu_0 \varepsilon_0}} \equiv \text{speed of light}$$

$$Z_0 \equiv \sqrt{\frac{\mu_0}{\varepsilon_0}} \equiv \text{wave impedance}$$

(1.6)

$\mu_0 \equiv$ permeability of free space

$\varepsilon_0 \equiv$ permittivity of free space

$\gamma = \frac{s}{c} \equiv$ propagation constant of free space

3

To complete the definitions of the terms in (2.1) we have for electric-dipole sensors

$$E_{ref}(t) \equiv \text{incident electric field parallel to } \vec{A}_{e_{eq}}$$

$$= \vec{E}_{inc}(t) \cdot \vec{1}_{e_{eq}}$$

$$\vec{1}_{e_{eq}} \equiv \text{unit vector in } \vec{A}_{e_{eq}} \text{ direction}$$

$$= \frac{\vec{A}_{e_{eq}}}{A_{e_{eq}}}$$

$$A_{e_{eq}} = |\vec{A}_{e_{eq}}|$$

(1.7)

$$H_{ref}(t) \equiv \frac{1}{Z_0} E_{ref}(t)$$

and for magnetic-dipole sensors

$$H_{ref}(t) \equiv \text{incident magnetic field parallel to } \vec{A}_{h_{eq}}$$

$$= \vec{H}_{inc}(t) \cdot \vec{1}_{h_{eq}}$$

$$\vec{1}_{h_{eq}} \equiv \text{unit vector in } \vec{A}_{h_{eq}} \text{ direction}$$

$$= \frac{\vec{A}_{h_{eq}}}{A_{h_{eq}}}$$

(1.8)

$$A_{h_{eq}} = |\vec{A}_{h_{eq}}|$$

$$E_{ref}(t) \equiv Z_0 H_{ref}(t)$$

b. Figure of merit in terms of power

As discussed in [6] there are limitations in $\Lambda^{(V)}$ and $\Lambda^{(I)}$ because ideal transformers can arbitrarily increase voltage or current if the load impedance Z_c is changed correspondingly. This difficulty is avoided by defining

$$\Lambda \equiv [\Lambda^{(V)}\Lambda^{(I)}]^{\frac{1}{2}}$$

$$= \left| \frac{\tilde{V}_{ideal}(j\omega_c)}{\tilde{E}_{ref}(j\omega_c)} \frac{\tilde{I}_{ideal}(j\omega_c)}{\tilde{H}_{ref}(j\omega_c)} \right|^{\frac{1}{2}} \frac{1}{\ell_c}$$

$$= \left(\frac{Z_0}{Z_c}\right)^{\frac{1}{2}} \left| \frac{\tilde{V}_{ideal}(j\omega_c)}{\tilde{E}_{ref}(j\omega_c)} \right| \frac{1}{\ell_c}$$

$$= \left(\frac{Z_c}{Z_0}\right)^{\frac{1}{2}} \left| \frac{\tilde{I}_{ideal}(j\omega_c)}{\tilde{H}_{ref}(j\omega_c)} \right| \frac{1}{\ell_c} \tag{1.9}$$

For electric-dipole sensors we then have

$$\Lambda^{(V)} = \frac{Z_c}{Z_0} A_{e_{eq}} \ell_c^{-2}$$

$$\Lambda^{(I)} = A_{e_{eq}} \ell_c^{-2}$$

$$\Lambda = \left(\frac{Z_c}{Z_0}\right)^{\frac{1}{2}} A_{e_{eq}} \ell_c^{-2} \tag{1.10}$$

and for magnetic-dipole sensors we have

$$\Lambda^{(V)} = A_{e_{eq}} \ell_c^{-2}$$

$$\Lambda^{(I)} = \frac{Z_o}{Z_c} A_{h_{eq}} \ell_c^{-2}$$

$$\Lambda = \left(\frac{Z_o}{Z_c}\right)^{\frac{1}{2}} A_{h_{eq}} \ell_c^{-2} \tag{1.11}$$

One can also interpret Λ in terms of power. Define

$$P_{ideal}(\omega) \equiv |\tilde{V}_{ideal}(j\omega)\ \tilde{I}_{ideal}(j\omega)| \tag{1.12}$$

for the case of

$$\tilde{V}_{ideal}(s) = Z_c \tilde{I}_{ideal}(s) \tag{1.13}$$

for which the voltage and current are in phase. In this case (1.12) corresponds to peak CW power in the quasi-static regime. Correspondingly define

$$S_{ref}(\omega) = |\tilde{E}_{ref}(j\omega)\ \tilde{H}_{ref}(j\omega)| \tag{1.14}$$

for the case of a plane wave with

$$\tilde{E}_{ref}(s) = Z_o \tilde{H}_{ref}(s) \tag{1.15}$$

for which the electric and magnetic fields are in phase. In this case (1.14) is related to a component of the Poynting vector. With these definitions we have

$$\Lambda \equiv \left[\frac{P_{ideal}(\omega_c)}{S_{ref}(\omega_c)}\right]^{\frac{1}{2}} \frac{1}{\ell_c} \tag{1.16}$$

Thus the figure of merit can be interpreted in terms of the ratio of the output power (into the load) to the input power per unit area in the incident electromagnetic wave, evaluated at the upper frequency response.

Interpreting these results we have for electric-dipole sensors

$$\Lambda = \frac{[P_{ideal}(\omega_c)]^{\frac{1}{2}}}{|\tilde{E}_{ref}(j\omega_c)|} \frac{Z_o^{\frac{1}{2}}}{\ell_c} \tag{1.17}$$

6

and for magnetic-dipole sensors

$$\Lambda = \frac{[P_{ideal}(\omega_c)]^{\frac{1}{2}}}{|\tilde{H}_{ref}(j\omega_c)|} \; \frac{1}{Z_o^{\frac{1}{2}}\ell_c}$$ (1.18)

In this form each type of sensor has its figure of merit cast in terms of its frequency-response parameter (ℓ_c), appropriate reference field component, and power delivered to a resistive load. Later in this note this form will be important because our ideal sensor does not have specified terminals, but absorbed power can still be considered for an idealized distributed sensor.

II.   Idealized Spherical Sensors

Figure 2.1 shows an idealized spherical sensor centered on $\vec{r} = \vec{0}$. This sensor is an impedance sheet of sheet-impedance value $\tilde{Z}_s(s)$ located on $r = |\vec{r}| = a$.

Since it is desirable to have the upper frequency response independent of the direction of incidence, $\vec{1}_I$, then one might desire the transit time of the incident wave across the sensor to be independent of $\vec{1}_1$ which can vary over 4π steradians. This leads to a spherical geometry.

Since spherical coordinates (r,θ,ϕ) as in fig. 2.1 are one of the few coordinate systems in which solutions of Maxwell's equations are separable, one has another reason for a spherical sensor. In particular let us assume a sheet impedance $\tilde{Z}_s(s)$ (a scalar) which is located on a spherical surface given by $r = a$ and which is independent of (θ,ϕ) on which to base our idealized sensor. This sheet impedance relates tangential electric field and surface current density as

$$\overleftrightarrow{1}_t \cdot \vec{\tilde{E}}(a,\theta,\phi,s) = \tilde{Z}_s(s)\vec{\tilde{J}}_s(\theta,\phi,s)$$

$$\overleftrightarrow{1}_t = \overleftrightarrow{1} - \vec{1}_r\vec{1}_r \equiv \text{transverse dyad}$$

$$\overleftrightarrow{1} \equiv \text{identity dyad} \tag{2.1}$$

$$\vec{1}_u \equiv \text{unit vector for u coordinate}$$

The surface current density is in turn related to the magnetic field via

$$\vec{1}_r \times [\vec{\tilde{H}}(a+,\theta,\phi,s) - \vec{\tilde{H}}(a-,\theta,\phi,s)] = \vec{\tilde{J}}_s(\theta,\phi,s) \tag{2.2}$$

A more general approach would be to use a volume-distributed loading instead of restricting it to a surface. Spherical symmetry can still be maintained by a conductivity and/or permittivity of the form $\tilde{\sigma}(r,s) + s\tilde{\varepsilon}(r,s)$, i.e., not a function of (θ,ϕ). Perhaps this can be explored in the future.

Of course a practical sensor will at best only approximate such a spherical impedance sheet. The assembly of conductors and loads at ports (such as transmission lines) can at best approximate the ideal sensor in some

Figure 2.1. Idealized Spherical Sensor

average sense. As will be seen later, it is only certain of the spherical surface current modes that one wishes to couple to the sensor output. This will influence the design of practical sensors in a manner that makes the orientation of conductors "orthogonal" to unwanted modes. Symmetry will be quite important.

III. Electromagnetic Fields in Spherical Coordinates

This subject has been developed in terms of the complex-frequency or Laplace-transform variable in [5,12,13]. In terms of ω this has been developed in various texts.

Summarizing we have spherical harmonics

$$Y_{n,m,\begin{smallmatrix}e\\o\end{smallmatrix}}(\theta,\phi) = P_n^{(m)}(\cos(\theta)) \left\{ \begin{array}{c} \cos(m\phi) \\ \sin(m\phi) \end{array} \right\}$$

$$\vec{P}_{n,m,p}(\theta,\phi) = Y_{n,m,p}(\theta,\phi)\, \vec{1}_r$$

$$\vec{Q}_{n,m,p}(\theta,\phi) = \nabla_s Y_{n,m,p}(\theta,\phi) = \vec{1}_r \times \vec{R}_{n,m,p}(\theta,\phi)$$

(3.1)

$$\vec{Q}_{n,m,\begin{smallmatrix}e\\o\end{smallmatrix}}(\theta,\phi) = \vec{1}_\theta \frac{dP_n^{(m)}(\cos(\theta))}{d\theta} \left\{ \begin{array}{c} \cos(m\phi) \\ \sin(m\phi) \end{array} \right\} + \vec{1}_\phi \frac{P_n^{(m)}(\cos(\theta))}{\sin(\theta)} m \left\{ \begin{array}{c} -\sin(m\phi) \\ \cos(m\phi) \end{array} \right\}$$

$$\vec{R}_{n,m,p}(\theta,\phi) = \nabla_s \times \vec{P}_{n,m,p}(\theta,\phi) = -\vec{1}_r \times \vec{Q}_{n,m,p}(\theta,\phi)$$

$$\vec{R}_{n,m,\begin{smallmatrix}e\\o\end{smallmatrix}}(\theta,\phi) = \vec{1}_\theta \frac{P_n^{(m)}(\cos(\theta))}{\sin(\theta)} m \left\{ \begin{array}{c} -\sin(m\phi) \\ \cos(m\phi) \end{array} \right\} - \vec{1}_\phi \frac{dP_n^{(m)}(\cos(\theta))}{d\theta} \left\{ \begin{array}{c} \cos(m\phi) \\ \sin(m\phi) \end{array} \right\}$$

with the Legendre functions given by

$$P_n^{(m)}(\xi) \equiv (-1)^m (1 - \xi^2)^{m/2} \frac{d^m}{d\xi^m} P_n(\xi)$$

(3.2)

$$P_n(\xi) \equiv P_n^{(0)}(\xi) \equiv \frac{1}{2^n n!} \frac{d^n}{d\xi^n} [(\xi^2 - 1)^n]$$

These are used in constructing the spherical wave functions

$$\Xi_{n,m,p}^{(\ell)}(\gamma\vec{r}) = f_n^{(\ell)}(\gamma r) P_n^{(m)}(\theta,\phi)$$

11

$$\vec{L}_{n,m,p}^{(\ell)}(\gamma\vec{r}) = \frac{1}{\gamma} \nabla \Xi_{n,m,p}^{(\ell)}(\gamma\vec{r})$$

$$= f_n^{(\ell)}{}'(\gamma r)\ \vec{P}_{n,m,p}(\theta,\phi) + \frac{f_n^{(\ell)}(\gamma r)}{\gamma r}\ \vec{Q}_{n,m,p}(\theta,\phi)$$

$$\vec{M}_{n,m,p}^{(\ell)}(\gamma\vec{r}) = \nabla \times [\vec{r}\Xi_{n,m,p}^{(\ell)}(\gamma\vec{r})]$$

$$= -\gamma r \times \vec{L}_{n,m,p}^{(\ell)}(\gamma\vec{r}) = -\frac{1}{\gamma} \nabla \times \vec{N}_{n,m,p}^{(\ell)}(\gamma\vec{r})$$

$$= f_n^{(\ell)}(\gamma r)\ \vec{R}_{n,m,p}(\theta,\phi)$$

$$\vec{N}_{n,m,p}^{(\ell)}(\gamma\vec{r}) = \frac{1}{\gamma} \nabla \times \vec{M}_{n,m,p}^{(\ell)}(\gamma\vec{r})$$

$$= n(n+1)\ \frac{f_n^{(\ell)}(\gamma r)}{\gamma r}\ \vec{P}_{n,m,p}(\theta,\phi) + \frac{[\gamma r f_n^{(\ell)}(\gamma r)]'}{\gamma r}\ \vec{Q}_{n,m,p}(\theta,\phi)$$

(3.3)

The spherical Bessel functions are denoted by

$$f_n^{(1)}(\gamma r) = i_n(\gamma r)$$

$$f_n^{(2)}(\gamma r) = k_n(\gamma r)$$

(3.4)

with

$$i_n(\zeta) = \frac{e^{\zeta}}{2\zeta} \sum_{\beta=0}^{n} \frac{(n+\beta)!}{\beta!(n-\beta)!} (-2\zeta)^{-\beta} + (-1)^{n+1} \frac{e^{-\zeta}}{2\zeta} \sum_{\beta=0}^{n} \frac{(n+\beta)!}{\beta!(n-\beta)!} (2\zeta)^{-\beta}$$

$$k_n(\zeta) = \frac{e^{-\zeta}}{\zeta} \sum_{\beta=0}^{n} \frac{(n+\beta)!}{\beta!(n-\beta)!} (2\zeta)^{-\beta}$$

$$i_n(\zeta) = \frac{1}{2}[(-1)^{n+1} k_n(\zeta) + k_n(-\zeta)]$$

(3.5)

A prime is used to indicate a derivative with respect to the argument of a Bessel function. The propagation constant is

$$\gamma = [s\mu(\sigma + s\varepsilon)]^{\frac{1}{2}}$$

$$\mu \equiv \text{permeability}$$

$$\sigma \equiv \text{conductivity} \tag{3.6}$$

$$\varepsilon \equiv \text{permittivity}$$

For later use we have for particular Bessel-function representations

$$i_1(\zeta) = \frac{1}{2}\left\{ e^{\zeta}[\zeta^{-1} - \zeta^{-2}] + e^{-\zeta}[\zeta^{-1} + \zeta^{-2}] \right\}$$

$$= \zeta^{-1}\cosh(\zeta) - \zeta^{-2}\sinh(\zeta)$$

$$= \frac{\zeta}{3}[1 + O(\zeta^2)] \qquad \text{as } \zeta \to 0$$

$$k_1(\zeta) = e^{-\zeta}[\zeta^{-1} + \zeta^{-2}]$$

$$= \zeta^{-2}[1 + O(\zeta^2)] \qquad \text{as } \zeta \to 0$$

$$\tag{3.7}$$

$$[\zeta i_1(\zeta)]' = \frac{1}{2}\left\{ e^{\zeta}[1 - \zeta^{-1} + \zeta^{-2}] - e^{-\zeta}[1 + \zeta^{-1} + \zeta^{-2}] \right\}$$

$$= [1 + \zeta^{-2}]\sinh(\zeta) - \zeta^{-1}\cosh(\zeta)$$

$$= \frac{2}{3}\zeta[1 + O(\zeta^2)] \qquad \text{as } \zeta \to 0$$

$$[\zeta k_1(\zeta)]' = -e^{-\zeta}[1 + \zeta^{-1} + \zeta^{-2}]$$

$$= -\zeta^{-2}[1 + O(\zeta^2)] \qquad \text{as } \zeta \to 0$$

Associated particular Legendre-function representations are

$$P_1^{(0)}(\xi) = \xi \quad , \quad P_1^{(0)}(\cos(\theta)) = \cos(\theta)$$

$$\tag{3.8}$$

$$P_1^{(1)}(\xi) = -(1 - \xi^2)^{\frac{1}{2}} \quad , \quad P_1^{(1)}(\cos(\theta)) = -\sin(\theta)$$

13

Particular spherical harmonics are

$$\vec{Q}_{1,0,{}^e_o} = -\vec{1}_\theta \sin(\theta) \begin{Bmatrix} 1 \\ 0 \end{Bmatrix}$$

$$\vec{Q}_{1,1,{}^e_o} = -\vec{1}_\theta \cos(\theta) \begin{Bmatrix} \cos(\phi) \\ \sin(\phi) \end{Bmatrix} - \vec{1}_\phi \begin{Bmatrix} -\sin(\phi) \\ \cos(\phi) \end{Bmatrix}$$

$$\vec{R}_{1,0,{}^e_o} = \vec{1}_\phi \sin(\theta) \begin{Bmatrix} 1 \\ 0 \end{Bmatrix}$$

$$\vec{R}_{1,1,{}^e_o} = -\vec{1}_\theta \begin{Bmatrix} -\sin(\phi) \\ \cos(\phi) \end{Bmatrix} + \vec{1}_\phi \cos(\theta) \begin{Bmatrix} \cos(\phi) \\ \sin(\phi) \end{Bmatrix}$$

(3.9)

IV. Plane Waves in Spherical Coordinates

Define a set of orthogonal (right-handed) unit vectors by

$$\vec{1}_1 = \sin(\theta_1)\cos(\phi_1)\vec{1}_x + \sin(\theta_1)\sin(\phi_1)\vec{1}_y + \cos(\theta_1)\vec{1}_z$$

$$\vec{1}_2 = -\cos(\theta_1)\cos(\phi_1)\vec{1}_x - \cos(\theta_1)\sin(\phi_1)\vec{1}_y + \sin(\theta_1)\vec{1}_z$$

$$\vec{1}_3 = \sin(\phi_1)\vec{1}_x - \cos(\phi_1)\vec{1}_y$$

(4.1)

Here $\vec{1}_1$ is the direction of propagation and $\vec{1}_2$ and $\vec{1}_3$ are mutually orthogonal unit vectors, each orthogonal to $\vec{1}_1$ to indicate the polarization of the electromagnetic fields in the incident plane wave. As indicated in fig. 4.1, θ_1 is the angle of $\vec{1}_1$ with respect to the z axis and ϕ_1 is the angle of its projection on the x,y plane with respect to the x axis. For convenience $\vec{1}_2$ is chosen in a plane parallel to $\vec{1}_1$ and the z axis (E or TM polarization if the electric field is parallel to $\vec{1}_2$) while $\vec{1}_3$ is then parallel to the x,y plane (H or TE polarization if the electric field is parallel to $\vec{1}_3$). In (4.1) we can use the relations between Cartesian and spherical coordinates

$$x = r \sin(\theta)\cos(\phi)$$

$$y - r \sin(\theta)\sin(\phi)$$

$$z = r \cos(\theta)$$

(4.2)

$$\vec{1}_x = \sin(\theta)\cos(\phi)\vec{1}_r + \cos(\theta)\cos(\phi)\vec{1}_\theta - \sin(\phi)\vec{1}_\theta$$

$$\vec{1}_y = \sin(\theta)\sin(\phi)\vec{1}_r + \cos(\theta)\sin(\phi)\vec{1}_\theta + \cos(\phi)\vec{1}_\phi$$

$$\vec{1}_z = \cos(\theta)\vec{1}_r - \sin(\theta)\vec{1}_\theta$$

to express the incident-wave unit vectors in terms of (θ_1,ϕ_1) and (θ,ϕ).
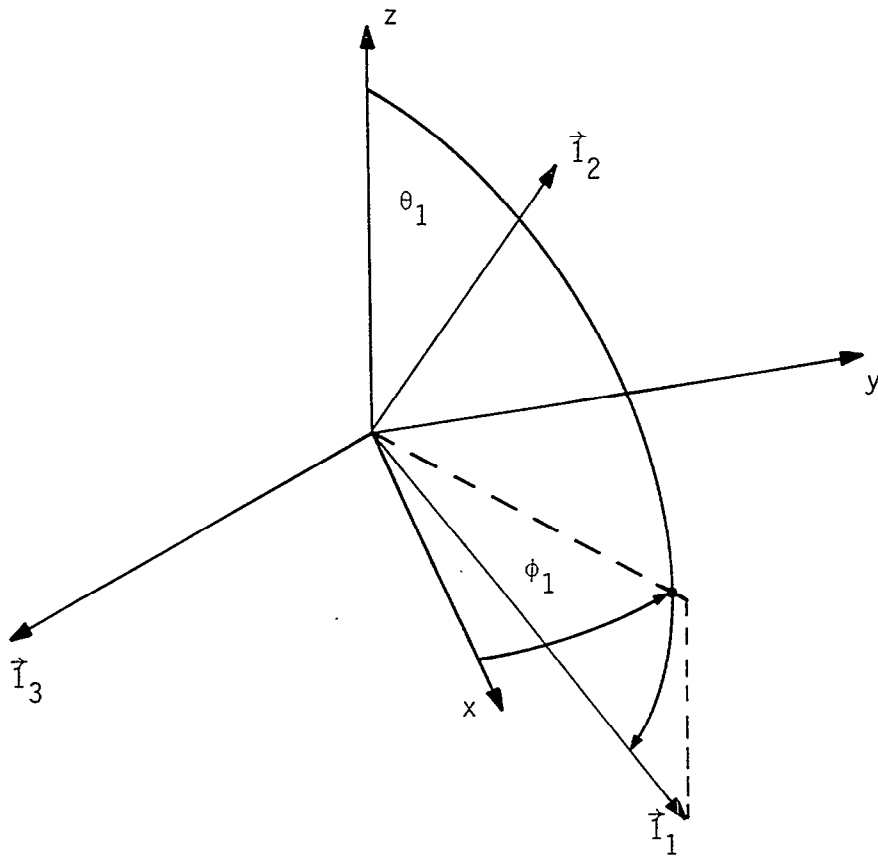
Next we have the result for a dyadic plane wave [4,12,15]

15

Figure 4.1.   Unit Vectors for Plane Wave

$$\vec{1} e^{-\gamma \vec{1}_1 \cdot \vec{r}} = \sum_{n=0}^{\infty} \sum_{m=0}^{n} \sum_{p=e,0} [2 - 1_{0,m}](-1)^n (2n+1) \frac{(n-m)!}{(n+m)!}$$

$$\left\{ -\vec{P}_{n,m,p}(\theta_1,\phi_1) \vec{L}^{(1)}_{n,m,p}(\gamma\vec{r}) \right.$$

(4.3)

$$\left. + \frac{1}{n(n+1)} \left[\vec{R}_{n,m,p}(\theta_1,\phi_1) \vec{M}^{(1)}_{n,m,\ell}(\gamma\vec{r}) - \vec{Q}_{n,m,p}(\theta_1,\phi_1) \vec{N}^{(1)}_{n,m,\ell}(\gamma\vec{r}) \right] \right\}$$

where for $n = 0$ the summation does not extend over the identically zero $\vec{Q}$, $\vec{R}$, $\vec{M}$, and $\vec{N}$ functions. For vector plane waves we have the set of orthogonal unit vectors $\{\vec{1}_1, \vec{1}_2, \vec{1}_3\}$. In free space, electromagnetic plane waves have both electric and magnetic fields orthogonal to $\vec{1}_1$ (as well as to each other). Thus only $\vec{1}_2$ and $\vec{1}_3$ are of concern. This removes the presence of the $\vec{L}$ functions in the expansion (since plane waves have zero-divergence fields). Taking dot products of $\vec{1}_2$ and $\vec{1}_3$ with (4.3) gives

$$\vec{1}_2 e^{-\gamma \vec{1}_1 \cdot \vec{r}} = \sum_{n=1}^{\infty} \sum_{m=0}^{n} \sum_{p=e,0} \left[a'_{n,m,p} \vec{M}^{(1)}_{n,m,p}(\gamma\vec{r}) + b'_{n,m,p} \vec{N}^{(1)}_{n,m,p}(\gamma\vec{r}) \right]$$

$$\vec{1}_3 e^{-\gamma \vec{1}_1 \cdot \vec{r}} = \sum_{n=1}^{\infty} \sum_{m=0}^{n} \sum_{p=e,0} \left[b'_{n,m,p} \vec{M}^{(1)}_{n,m,p}(\gamma\vec{r}) - a'_{n,m,p} \vec{N}^{(1)}_{n,m,p}(\gamma\vec{r}) \right]$$

(4.4)

$$a'_{n,m,\substack{e \\ 0}} = [2 - 1_{0,m}](-1)^{n+1} \frac{2n+1}{n(n+1)} \frac{(n-m)!}{(n+m)!} m \frac{P_n^{(m)}(\cos(\theta_1))}{\sin(\theta_1)} \begin{Bmatrix} -\sin(m\phi_1) \\ \cos(m\phi_1) \end{Bmatrix}$$

$$b'_{n,m,\substack{e \\ 0}} = [2 - 1_{0,m}](-1)^n \frac{2n+1}{n(n+1)} \frac{(n-m)!}{(n+m)!} \frac{dP_n^{(m)}(\cos(\theta_1))}{d\theta_1} \begin{Bmatrix} \cos(m\phi_1) \\ \sin(m\phi_1) \end{Bmatrix}$$

Particular coefficients of interest are

17

$$a'_{1,0,\underset{o}{e}} = 0$$

$$a'_{1,1,\underset{o}{e}} = \frac{3}{2} \frac{P_1^{(1)}(\cos(\theta_1))}{\sin(\theta_1)} \begin{Bmatrix} -\sin(\phi_1) \\ \cos(\phi_1) \end{Bmatrix} = -\frac{3}{2} \begin{Bmatrix} -\sin(\phi_1) \\ \cos(\phi_1) \end{Bmatrix}$$

$$b'_{1,0,\underset{o}{e}} = -\frac{3}{2} \frac{dP_1^{(0)}(\cos(\theta_1))}{d\theta_1} \begin{Bmatrix} 1 \\ 0 \end{Bmatrix} = \frac{3}{2} \sin(\theta_1) \begin{Bmatrix} 1 \\ 0 \end{Bmatrix}$$

$$b'_{1,1,\underset{o}{e}} = -\frac{3}{2} \frac{dP_1^{(1)}(\cos(\theta_1))}{d\theta_1} \begin{Bmatrix} \cos(\phi_1) \\ \sin(\phi_1) \end{Bmatrix} = \frac{3}{2} \cos(\theta_1) \begin{Bmatrix} \cos(\phi_1) \\ \sin(\phi_1) \end{Bmatrix}$$

(4.5)

18

V. Solution of Scattering Problem

Let us define our incident plane wave as an E wave (TM wave)

$$\tilde{\vec{E}}_{inc}(\vec{r},s) = E_0 \vec{1}_2 \, e^{-\gamma \vec{1}_1 \cdot \vec{r}}$$

$$\tilde{\vec{H}}_{inc}(\vec{r},s) = \frac{E_0}{Z_0} \vec{1}_3 \, e^{-\gamma \vec{1}_1 \cdot \vec{r}} \tag{5.1}$$

One can also define an H wave (TE wave) in a similar way. However, utilizing the symmetry of the spherical sensor one can move the observation position (or function) on the sphere by a rotation so as to obtain all possible plane waves with respect to an observer.

Expand the fields for $r < a$ as

$$\tilde{\vec{E}}_{in}(\vec{r},s) = E_0 \sum_{n=1}^{\infty} \sum_{m=0}^{n} \sum_{p=e,0} \left[a''_{n,m,p} \vec{M}^{(1)}_{n,m,p}(\gamma\vec{r}) + b''_{n,m,p} \vec{N}^{(1)}_{n,m,p}(\gamma\vec{r}) \right]$$

$$\tag{5.2}$$

$$\tilde{\vec{H}}_{in}(\vec{r},s) = \frac{E_0}{Z_0} \sum_{n=1}^{\infty} \sum_{m=0}^{n} \sum_{p=e,0} \left[b''_{n,m,p} \vec{M}^{(1)}_{n,m,p}(\gamma\vec{r}) - a''_{n,m,p} \vec{N}^{(1)}_{n,m,p}(\gamma\vec{r}) \right]$$

and expand the scattered fields for $r > a$ as

$$\tilde{\vec{E}}_{sc}(\vec{r},s) = E_0 \sum_{n=1}^{\infty} \sum_{m=0}^{n} \sum_{p=e,0} \left[a'''_{n,m,p} \vec{M}^{(2)}_{n,m,p}(\gamma\vec{r}) + b'''_{n,m,p} \vec{N}^{(2)}_{n,m,p}(\gamma\vec{r}) \right]$$

$$\tag{5.3}$$

$$\tilde{\vec{H}}_{sc}(\vec{r},s) = \frac{E_0}{Z_0} \sum_{n=1}^{\infty} \sum_{m=0}^{n} \sum_{p=e,0} \left[b'''_{n,m,p} \vec{M}^{(2)}_{n,m,p}(\gamma\vec{r}) - a'''_{n,m,p} \vec{N}^{(2)}_{n,m,p}(\gamma\vec{r}) \right]$$

Matching boundary conditions on $r = a$, continuity of tangential electric field combines with (2.1) and (2.2) to give

$$\overleftrightarrow{1}_t \cdot \left[\tilde{\vec{E}}_{inc}(1+,\theta,\phi,s) + \tilde{\vec{E}}_{sc}(a+,\theta,\phi,s) \right] = \overleftrightarrow{1}_t \cdot \tilde{\vec{E}}_{in}(a-,\theta,\phi,s)$$

$$= \tilde{Z}_s(s) \tilde{\vec{J}}_s(\theta,\phi,s)$$

$$= \tilde{Z}_s(s) \vec{1}_r \times \left[\tilde{\vec{H}}_{inc}(a+,\theta,\phi,s) + \tilde{\vec{H}}_{sc}(a+,\theta,\phi,s) - \tilde{\vec{H}}_{in}(a-,\theta,\phi,s) \right]$$

$$\tag{5.4}$$

Substituting the series representations for the fields and noting the orthogonalities of the functions (tangential components) on the surface of the sphere gives equations for the coefficients as

$$a'_{n,m,p} i_n(\gamma a) + a'''_{n,m,p} k_n(\gamma a) = a''_{n,m,p} i_n(\gamma a)$$

$$= \frac{\tilde{Z}_s(s)}{Z_0} \left\{ a'_{n,m,p} \frac{[\gamma a i_n(\gamma a)]'}{\gamma a} + a'''_{n,m,p} \frac{[\gamma a k_n(\gamma a)]'}{\gamma a} - a''_{n,m,p} \frac{[\gamma a i_n(\gamma a)]'}{\gamma a} \right\}$$

$$(5.5)$$

$$b'_{n,m,p} \frac{[\gamma a i_n(\gamma a)]'}{\gamma a} + b'''_{n,m,p} \frac{[\gamma a k_n(\gamma a)]'}{\gamma a} = b''_{n,m,p} \frac{[\gamma a i_n(\gamma a)]'}{\gamma a}$$

$$= \frac{\tilde{Z}_s(s)}{Z_0} \left\{ b'_{n,m,p} i_n(\gamma a) + b'''_{n,m,p} k_n(\gamma a) - b''_{n,m,p} i_n(\gamma a) \right\}$$

Eliminating the a''' and b''' coefficients gives

$$0 = a'_{n,m,p} \frac{\tilde{Z}_s(s)}{Z_0} \left\{ i_n(\gamma a) \frac{[\gamma a k_n(\gamma a)]'}{\gamma a} - k_n(\gamma a) \frac{[\gamma a i_n(\gamma a)]'}{\gamma a} \right\}$$

$$+ a''_{n,m,p} \left\{ \frac{-\tilde{Z}_s(s)}{Z_0} \left[i_n(\gamma a) \frac{[\gamma a k_n(\gamma a)]'}{\gamma a} - k_n(\gamma a) \frac{[\gamma a i_n(\gamma a)]'}{\gamma a} \right] + k_n(\gamma a) i_n(\gamma a) \right\}$$

$$0 = b'_{n,m,p} \frac{\tilde{Z}_s(s)}{Z_0} \left\{ k_n(\gamma a) \frac{[\gamma a i_n(\gamma a)]'}{\gamma a} - i_n(\gamma a) \frac{[\gamma a k_n(\gamma a)]'}{\gamma a} \right\}$$

$$+ b''_{n,m,p} \left\{ \frac{-Z_s(s)}{Z_0} \left[k_n(\gamma a) \frac{[\gamma a i_n(\gamma a)]'}{\gamma a} - i_n(\gamma a) \frac{[\gamma a k_n(\gamma a)]'}{\gamma a} \right] \right.$$

$$\left. + \frac{[\gamma a k_n(\gamma a)]'[\gamma a i_n(\gamma a)]'}{(\gamma a)^2} \right\}$$

Applying the Wronskian relation [5]

$$W\{\zeta i_n(\zeta), \zeta k_n(\zeta)\} = \zeta i_n(\zeta)[\zeta k_n(\zeta)]' - [\zeta i_n(\zeta)]' \zeta k_n(\zeta) = -1 \qquad (5.7)$$

20

gives solutions for the a" and b" coefficients as

$$a''_{n,m,p} = a'_{n,m,p} \left\{ 1 + \frac{Z_0}{\tilde{Z}_s(s)} (\gamma a)^2 \, i_n(\gamma a) k_n(\gamma a) \right\}^{-1}$$

$$b''_{n,m,p} = b'_{n,m,p} \left\{ 1 - \frac{Z_0}{\tilde{Z}_s(s)} [\gamma a i_n(\gamma a)]' [\gamma a k_n(\gamma a)]' \right\}^{-1}$$

VI.   Surface Current Density

Now the surface current density is

$$\tilde{\vec{J}}_s(\theta,\phi,s) = \frac{1}{\tilde{Z}_s(s)} \overleftrightarrow{1}_t \cdot \tilde{\vec{E}}(a,\theta,\phi,s)$$

$$= \frac{E_0}{\tilde{Z}_s(s)} \sum_{n=1}^{\infty} \sum_{m=0}^{n} \sum_{p=e,0} \left[a''_{n,m,p} \overleftrightarrow{1}_t \cdot \vec{M}^{(1)}_{n,m,p}(\gamma a \vec{1}_r) + b''_{n,m,p} \overleftrightarrow{1}_t \cdot \vec{N}^{(1)}_{n,m,p}(\gamma a \vec{1}_r) \right]$$

$$= \frac{E_0}{\tilde{Z}_s(s)} \sum_{n=1}^{\infty} \sum_{m=0}^{n} \sum_{p=e,0} \left[a''_{n,m,p} i_n(\gamma a) \vec{R}_{n,m,p}(\theta,\phi) \right.$$

$$\left. + b''_{n,m,p} \frac{[\gamma a i_n(\gamma a)]'}{\gamma a} \vec{Q}_{n,m,p}(\theta,\phi) \right] \tag{6.1}$$

At low frequencies the electric- and magnetic-dipole terms (n=1) are of course the dominant terms, as can be seen from the behavior of the spherical Bessel functions for small argument. Including only such terms we have

$$\tilde{\vec{J}}_s^{(1)}(\theta,\phi,s) = \frac{E_0}{Z_0} \sum_{m=0}^{1} \sum_{p=e,0} \left[\tilde{f}_h(s) a'_{1,m,p} \vec{R}_{1,m,p}(\theta,\phi) + \tilde{f}_e(s) b'_{n,m,p} \vec{Q}_{1,m,p}(\theta,\phi) \right] \tag{6.2}$$

where the superscript 1 on the surface current density indicates the dipole part. In this form we have the important dipole coefficients (electric and magnetic, respectively) relating the surface current density to the incident fields as

$$\tilde{f}_e(s) = \frac{Z_0}{\tilde{Z}_s(s)} \frac{[\gamma a i_n(\gamma a)]'}{\gamma a} \left\{ 1 - \frac{Z_0}{\tilde{Z}_s(s)} [\gamma a i_1(\gamma a)]' [\gamma a k_1(\gamma a)]' \right\}^{-1} \tag{6.3}$$

$$\tilde{f}_h(s) = \frac{Z_0}{\tilde{Z}_s(s)} i_1(\gamma a) \left\{ 1 + \frac{Z_0}{\tilde{Z}_s(s)} (\gamma a)^2 i_1(\gamma a) k_1(\gamma a) \right\}^{-1}$$

Then split this dipole part of the surface current density into electric and magnetic parts as

$$\tilde{\vec{J}}_s^{(1)}(\theta,\phi,s) = \tilde{\vec{J}}_s^{(e)}(\theta,\phi,s) + \tilde{\vec{J}}_s^{(h)}(\theta,\phi,s)$$

$$\tilde{\vec{J}}_s^{(e)}(\theta,\phi,s) = \frac{E_0}{Z_0} \tilde{f}_e(s) \sum_{m=0}^{1} \sum_{p=e,0} b'_{1,m,p}(\theta_1,\phi_1)\, \vec{Q}_{1,m,p}(\theta,\phi)$$

$$\tilde{\vec{J}}_s^{(h)}(\theta,\phi,s) = \frac{E_0}{Z_0} \tilde{f}_h(s) \sum_{m=0}^{1} \sum_{p=e,0} a'_{1,m,p}(\theta_1,\phi_1)\vec{R}_{1,m,p}(\theta,\phi)$$

In order to better visualize these surface currents let us specialize the incident wave to a particular set of parameters as

$$\theta_1 = \frac{\pi}{2} \quad , \quad \phi_1 = 0$$

$$\vec{1}_1 = \vec{1}_x \quad , \quad \vec{1}_2 = \vec{1}_z \quad , \quad \vec{1}_3 = -\vec{1}_y$$

(6.4)

giving

$$\tilde{\vec{J}}_s^{(e)}(\theta,\phi,s) = \frac{E_0}{Z_0} \tilde{f}_e(s)\left[-\frac{3}{2}\sin(\theta)\vec{1}_\theta\right]$$

(6.5)

$$\tilde{\vec{J}}_s^{(h)}(\theta,\phi,s) = \frac{E_0}{Z_0} \tilde{f}_h(s)\left[\frac{3}{2}\cos(\phi)\vec{1}_\theta - \frac{3}{2}\cos(\theta)\sin(\phi)\vec{1}_\phi\right]$$

Figure 6.1 illustrates the surface-current-density pattern for these electric- and magnetic-dipole terms on the spherical sensor. The electric term has the current density oriented in the θ direction proportional to sin(θ); note the symmetry with respect to the z axis including surface-current-density direction in a plane through the z axis and independent of the rotation of this plane (independent of φ). The magnetic term has the current density oriented parallel to the xz plane (or orthogonal to the y axis) proportional to the sine of the angle from the y axis; note the symmetry with respect to the y axis including

23
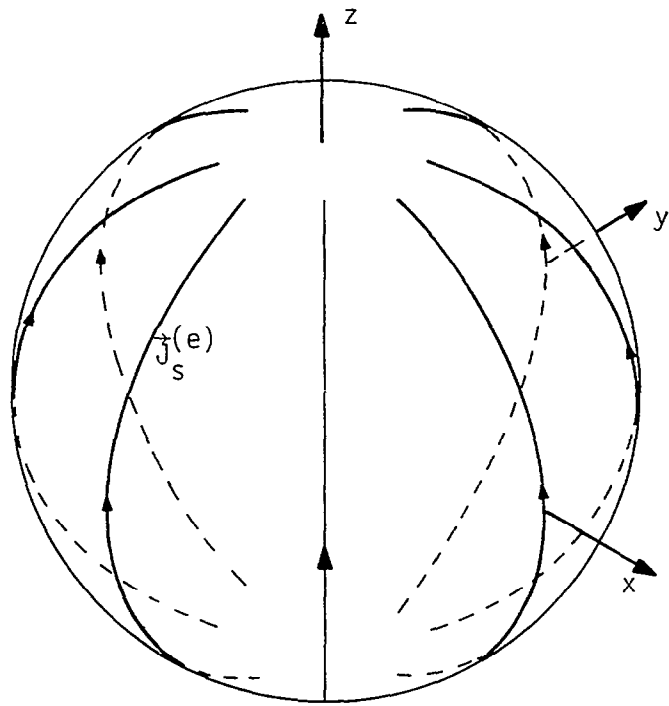
A. Electric-dipole pattern
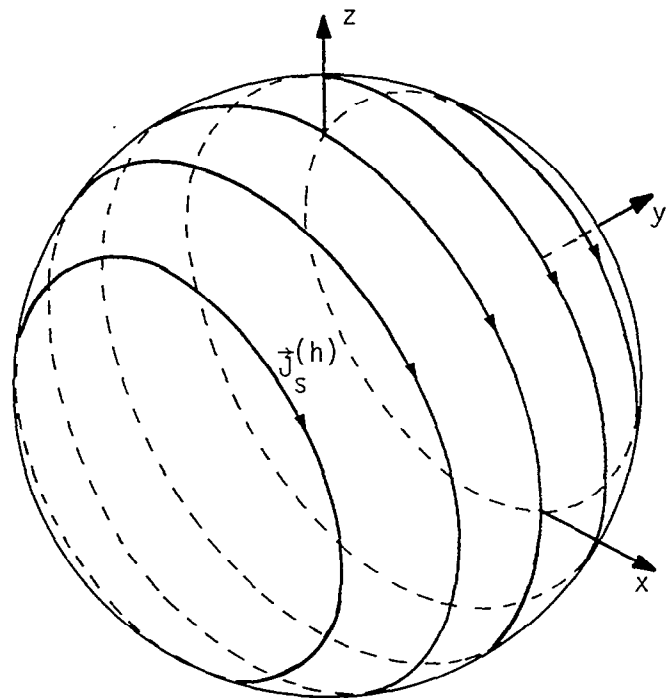
B. Magnetic-dipole pattern

Figure 6.1. Surface-Current-Density Distributions for Dipole Terms

surface-current-density direction orthogonal to a plane through the y axis and independent of the rotation of this plane (independent of the angle of the plane with respect to x or z axes).

A limiting case of interest for these results is for $\tilde{Z}_s(s) = 0$, i.e., a perfectly conducting sphere. In this case we have

$$\tilde{f}_e(s) = -\{\gamma a[\gamma a k_1(\gamma a)]'\}^{-1}$$

$$= \gamma a[1 + O((\gamma a)^2)] \qquad \text{as } s \to 0$$

$$\tilde{f}_h(s) = \{(\gamma a)^2 k_1(\gamma a)\}^{-1}$$

$$= 1 + O((\gamma a)^2) \qquad \text{as } s \to 0$$

(6.6)

The electric term is interpretable in terms of the surface charge density by the equation of continuity

$$\nabla_s \cdot \vec{J}_s^{(e)}(\theta,\phi) = -s\tilde{\rho}_s(\theta,\phi)$$

(6.7)

giving

$$\tilde{\rho}_s(\theta,\phi) = -\frac{1}{s} \frac{1}{a \sin(\theta)} \frac{\partial}{\partial\theta} [\sin(\theta) J_{s_\theta}^{(e)}(\theta,\phi,s)]$$

$$= \frac{E_0}{Z_0} \tilde{f}_e(s) \frac{3}{sa} \cos(\theta)$$

$$= 3\varepsilon_0 E_0 \frac{\tilde{f}_e(s)}{\gamma a} \cos(\theta)$$

$$= 3\varepsilon_0 E_0 \cos(\theta) \qquad \text{as } s \to 0$$

(6.8)

This shows the enhancement of the electric field by a factor of 3 in a uniform incident electric field at 2 appropriate "poles" of the sphere. The magnetic term gives

$$\vec{J}_s^{(h)}(\theta,\phi,s) = \frac{3}{2} \frac{E_0}{Z_0} [\cos(\phi)\vec{1}_\theta - \cos(\theta)\sin(\phi)\vec{1}_\phi]$$

This shows the enhancement of the surface current density by a factor of 3/2 in a uniform incident magnetic field at an appropriate "equator" given by the intersection of the xz plane with the sphere (corresponding to $\phi = 0, \pi$ with $0 \le \theta \le \pi$).

VII. Figure of Merit for Idealized Spherical Sensors

Section 1 discussed the figure of merit for such a sensor in terms of power delivered to a load and power in the incident field referred to the appropriate field component. Now let us apply (1.17) and (1.18) to our idealized spherical sensor.

Now it is our purpose to have the sensor output coupled to only one spherical mode for the surface current density, specifically $\tilde{J}_s^{(e)}$ or $\tilde{J}_s^{(h)}$ depending on the type of sensor (electric or magnetic) under consideration.

For the purposes of this note let us assume that

$$\tilde{Z}_s(s) \equiv R_s \tag{7.1}$$

i.e., that the sheet impedance is simply a frequency-independent sheet resistance. Furthermore let us assume that all the power from our desired surface-current-density mode delivered to R_s appears as power at the sensor output. Note that other assumptions are possible; $\tilde{Z}_s(s)$ could be a more general complex function of frequency and there could be some complex transfer function relating the surface-current-density mode to the sensor output. Perhaps these more general possibilities can be considered in the future.

For present purposes then let us take

$$
\begin{aligned}
P_{ideal}^{(e,h)}(\omega) &= |\tilde{V}_{ideal}(j\omega)\tilde{I}_{ideal}(j\omega)| \\
&= \int_S R_s \; \tilde{J}_{s_o}^{(e,h)}(\theta,\phi,j\omega) \cdot \tilde{J}_{s_o}^{(e,h)*}(\theta,\phi,j\omega) \; dS \\
&= R_s a^2 \int_0^{2\pi}\int_0^{\pi} \tilde{J}_{s_o}^{(e,h)}(\theta,\phi,j\omega) \cdot \tilde{J}_{s_o}^{(e,h)*}(\theta,\phi,j\omega) \; \sin(\theta) \; d\theta d\phi
\end{aligned}
\tag{7.2}
$$

where * indicates complex conjugate, the integral is over the surface of the sphere, and the extra subscript "o" indicates the leading term in the expansion of the "e" or "h" surface current density for low frequencies. For the electric sensor we have

$$P^{(e)}_{ideal}(\omega) = R_s a^2 \left[\frac{E_0}{Z_0} |\tilde{f}_{e_0}(j\omega)|\right]^2 \frac{9}{4} \int_0^{2\pi} \int_0^{\pi} \sin^3(\theta) \, d\theta d\phi$$

$$= 6\pi R_s a^2 \left[\frac{E_0}{Z_0} |\tilde{f}_{e_0}(j\omega)|\right]^2 \tag{7.3}$$

and for the magnetic sensor we have

$$P^{(h)}_{ideal}(\omega) = R_s a^2 \left[\frac{E_0}{Z_0} |\tilde{f}_{h_0}(j\omega)|\right]^2 \frac{9}{4} \int_0^{2\pi} \int_0^{\pi} [\sin(\theta)\cos^2(\phi) + \sin(\theta)\cos^2(\theta)\sin^2(\phi)] d\theta d\phi$$

$$= R_s a^2 \left[\frac{E_0}{Z_0} |\tilde{f}_{h_0}(j\omega)|\right]^2 \frac{9\pi}{4} \int_0^{\pi} [\sin(\theta) + \sin(\theta)\cos^2(\theta)] \, d\theta$$

$$= 6\pi R_s a^2 \left[\frac{E_0}{Z_0} |\tilde{f}_{h_0}(j\omega)|\right]^2 \tag{7.4}$$

Note the similarity of the final results of (7.3) and (7.4) with the only difference being the two dipole coefficients $\tilde{f}_{e_0}$ and $\tilde{f}_{h_0}$.

VIII. Electric-Dipole Response

Considering the electric-dipole coefficient function define

$$\tilde{f}_{e_0}(s) = \gamma a \tag{8.1}$$

so that

$$\frac{\tilde{f}_e(s)}{\tilde{f}_{e_0}(s)} \to 1 \qquad \text{as } s \to 0 \tag{8.2}$$

giving a normalized response function.

The departure of this function from unity at high frequencies can be used to define the upper frequency response. For low frequencies we have

$$e^{-\gamma a} \frac{\tilde{f}_e(s)}{\tilde{f}_{e_0}(s)} = \frac{1}{2(\gamma a)^2} \left\{ [(\gamma a)^{-2} - (\gamma a)^{-1} + 1] - e^{-2\gamma a}[(\gamma a)^{-2} + (\gamma a)^{-1} + 1] \right\}$$

$$\left\{ \frac{R_s}{Z_0} + \frac{1}{2}[(\gamma a)^{-2} - (\gamma a)^{-1} + 1] - e^{-2\gamma a}[(\gamma a)^{-2} + (\gamma a)^{-1} + 1] \right.$$

$$\left. [(\gamma a)^{-2} + (\gamma a)^{-1} + 1] \right\}^{-1}$$

$$= \frac{2}{3(\gamma a)^2} \left\{ \gamma a - (\gamma a)^2 + 0((\gamma a)^3) \right\}$$

$$\left\{ \frac{R_s}{Z_0} + \frac{2}{3}[\gamma a - (\gamma a)^2 + 0((\gamma a)^3)][(\gamma a)^{-2} + (\gamma a)^{-1} + 1] \right\}^{-1}$$

$$= (\gamma a)^{-2} \left\{ \frac{3}{2} \frac{R_s}{Z_0} (\gamma a)^{-2}[\gamma a + (\gamma a)^2 + 0((\gamma a)^3)] \right.$$

$$\left. + [(\gamma a)^{-2} + (\gamma a)^{-1} + 1] \right\}^{-1}$$

$$= \left\{ 1 + \left[\frac{3}{2} \frac{R_s}{Z_0} + 1 \right] \gamma a + 0((\gamma a)^2) \right\}^{-1} \qquad \text{as } s \to 0 \tag{8.3}$$

In this form one can identify a time constant

$$t_e = \left[\frac{3}{2}\frac{R_s}{Z_o} + 1\right]\frac{a}{c} = t_{RC} = t_t$$

$$t_{RC} \equiv \frac{3}{2} R_s \epsilon_o a \equiv \text{"low frequency" RC time constant}$$

(8.4)

$$t_t \equiv \frac{a}{c} \equiv \text{transit time for one radius}$$

Note the inclusion of a factor $e^{-\gamma a}$ with $\tilde{f}_e(s)$. This factor makes the time-domain form depart from the zero at $t = 0$ instead of $t = -a/c$. Expanding this normalized and delayed response function for low frequencies we can identify an RC time constant appropriate to a capacitive $\vec{E}$ or $\partial\vec{D}/\partial t$ sensor. However, this simple form only strictly applies for frequencies such that the sensor is electrically small. As the RC time approaches the transit time across the sensor (by decreasing R_s) then such a simple model of the response no longer applies; the sensor is becoming transit-time limited. This is reflected in the argument of the exponentials (γa) becoming comparable to unity.

Let us take our definition of upper frequency response as

$$\left| e^{-\frac{j\omega_c a}{c}} \frac{\tilde{f}_e(j\omega_c)}{\tilde{f}_{e_o}(j\omega_c)} \right| = \left| \frac{\tilde{f}_e(j\omega_c)}{\tilde{f}_{e_o}(j\omega_c)} \right| \equiv \frac{1}{\sqrt{2}}$$

(8.5)

At low frequencies we have found

$$\omega_c \simeq t_{RC}^{-1} = \left[\frac{3}{2} R_s \epsilon_o a\right]^{-1}$$

$$\frac{\omega_c a}{c} \simeq \left[\frac{c t_{RC}}{a}\right]^{-1} = \frac{2}{3}\frac{Z_o}{R_s}$$

(8.6)

Figure 8.1 is a graph of $e^{-\frac{j\omega a}{c}} \tilde{f}_e(j\omega)/\tilde{f}_{e_o}(j\omega)$ as a function of the normalized frequency $\omega a/c$ with selected values of Z_o/R_s as a parameter. Note for large values of Z_o/R_s the response exceeds unity for $\omega a/c$ a little less than 1.

Using (8.5) to define ω_c then fig. 8.2 has $\omega_c a/c$ as a function of Z_0/R_s. Note that the behavior of (8.6) is followed at low frequencies, but that $\omega_c a/c$ tends to about 1.27 as $Z_0/R_s \to \infty$.

Finally the figure of merit

$$\Lambda^{(e)} = \frac{\left[P^{(e)}_{ideal}(j\omega_c)\right]^{\frac{1}{2}}}{|\tilde{E}_{ref}(j\omega_c)|} Z_0^{\frac{1}{2}} \frac{\omega_c}{c}$$

$$= \left[6\pi \frac{R_s}{Z_0}\right]^{\frac{1}{2}} \frac{\omega_c a}{c} |\tilde{f}_{e_0}(j\omega_c)|$$

$$= \left[6\pi \frac{R_s}{Z_0}\right]^{\frac{1}{2}} \left[\frac{\omega_c a}{c}\right]^2$$

is plotted as a function of Z_0/R_s in fig. 8.3. As Z_0/R_s is increased we find a maximum given by

$$\Lambda^{(e)}_{max} \simeq 1.9378$$

$$\frac{Z_0}{R_s} \simeq 1.49$$
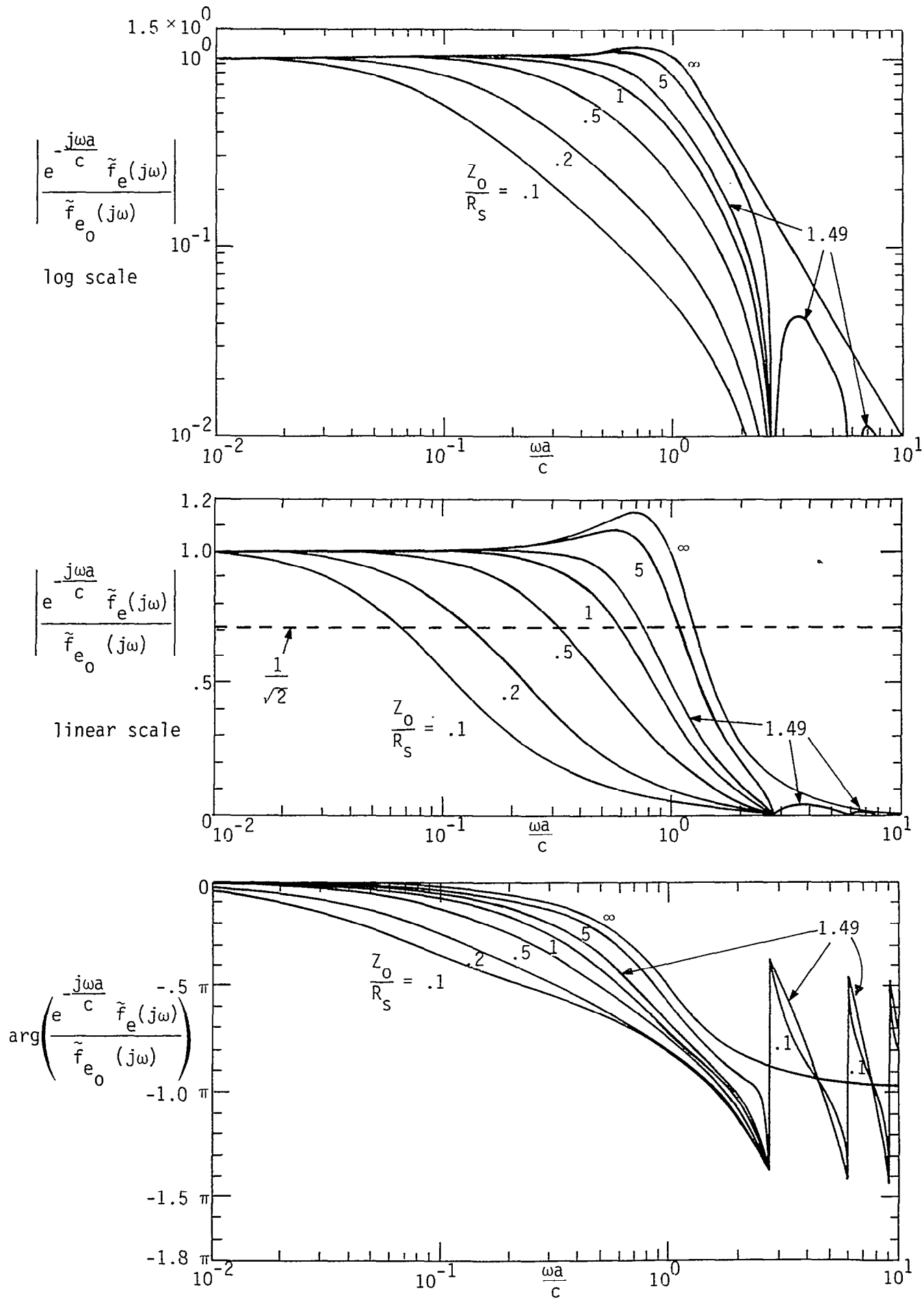
$$\frac{\omega_c a}{c} \simeq .769$$

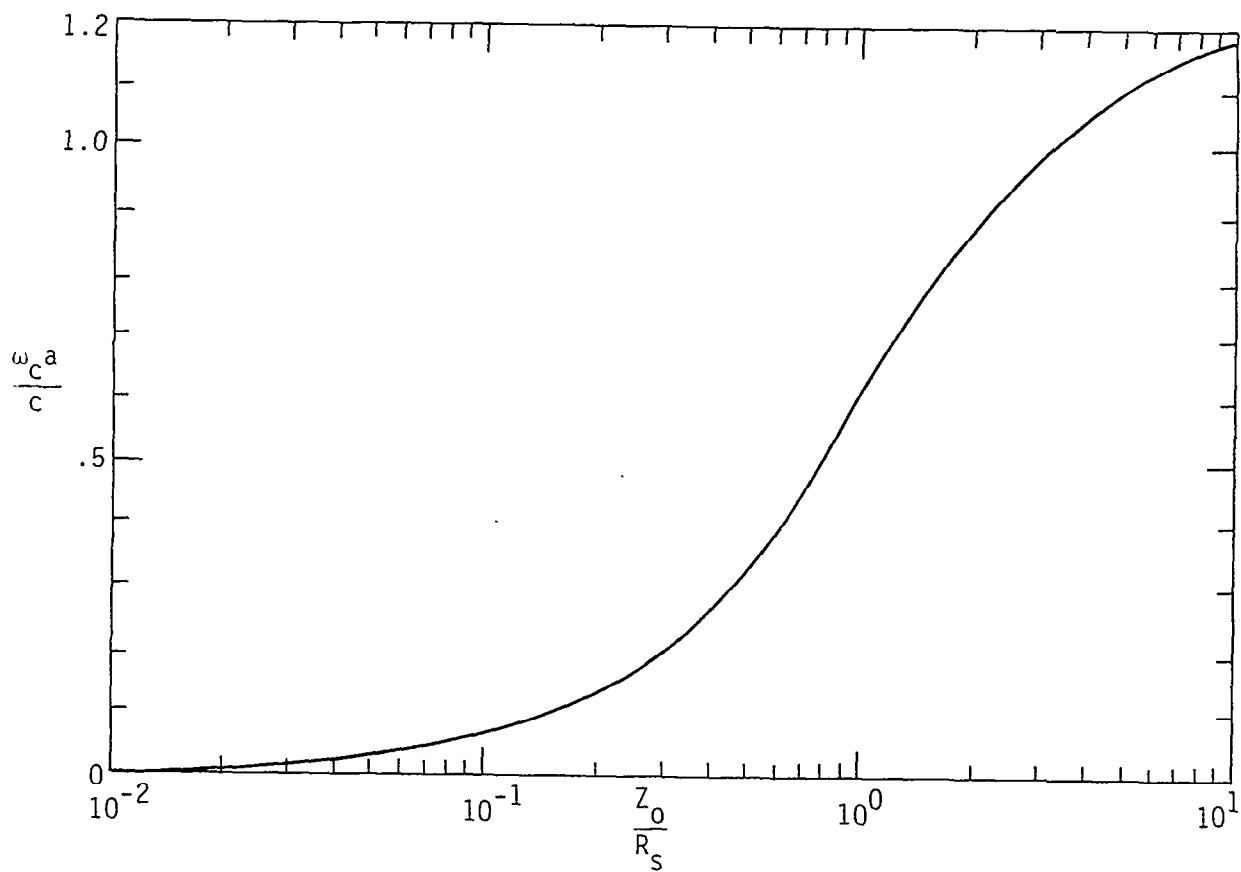Figure 8.1. Electric-Dipole Response Versus Frequency

32

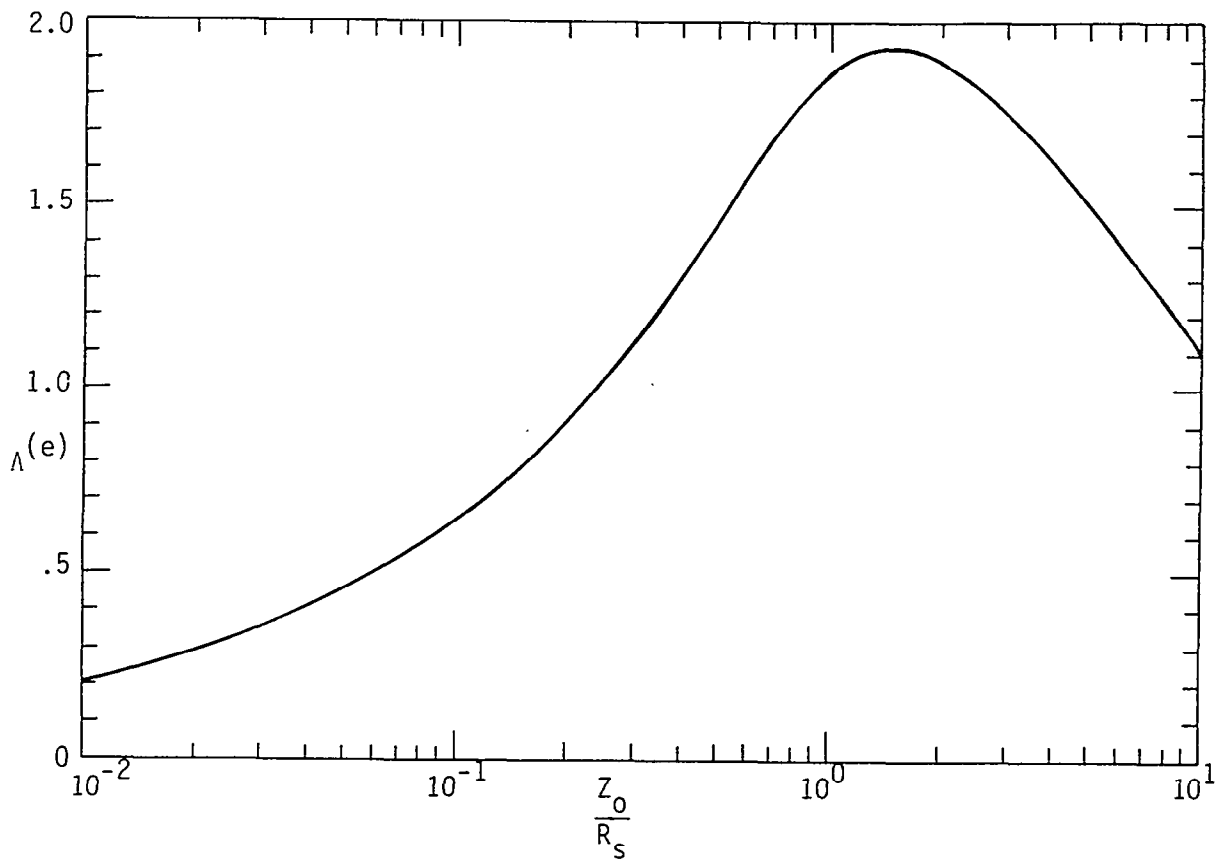Figure 8.2. Electric-Dipole Upper Frequency Response

Figure 8.3. Electric-Dipole Figure of Merit

IX. Magnetic-Dipole Sensor

Considering the magnetic-dipole coefficient define

$$\tilde{f}_{h_0}(s) = \frac{1}{3} \frac{Z_0}{R_s} \gamma a \tag{9.1}$$

so that

$$\frac{\tilde{f}_h(s)}{\tilde{f}_{h_0}(s)} \rightarrow 1 \qquad \text{as } s \rightarrow 0 \tag{9.2}$$

giving a normalized response function.

For low frequencies we have

$$e^{-\gamma a} \frac{\tilde{f}_h(s)}{\tilde{f}_{h_s}(s)} = \frac{3}{2\gamma a} \left\{ [-(\gamma a)^{-2} + (\gamma a)^{-1}] + e^{-2\gamma a}[(\gamma a)^{-2} + (\gamma a)^{-1}] \right\}$$

$$\left\{ 1 + \frac{Z_0}{R_s} \frac{(\gamma a)^2}{2} \left[[-(\gamma a)^{-2} + (\gamma a)^{-1}] + e^{-2\gamma a}[(\gamma a)^{-2} + (\gamma a)^{-1} + 1] \right] \right.$$

$$\left. [(\gamma a)^{-2} + (\gamma a)^{-2}] \right\}^{-1}.$$

$$= \frac{3}{2\gamma a} \left\{ \frac{2}{3} \gamma a - \frac{2}{3} (\gamma a)^2 + 0((\gamma a)^3) \right\}$$

$$\left\{ 1 + \frac{Z_0}{R_s} \frac{(\gamma a)^2}{2} \left[\frac{2}{3} \gamma a - \frac{2}{3} (\gamma a)^2 + 0((\gamma a)^3) \right] [(\gamma a)^{-2} + (\gamma a)^{-1}] \right\}^{-1}$$

$$= \left\{ [1 + \gamma a + 0((\gamma a)^2)] + \frac{Z_0}{R_s} \frac{(\gamma a)^3}{2} [(\gamma a)^{-2} + (\gamma a)^{-1}] \right\}^{-1}$$

$$= \left\{ 1 + \frac{1}{3} \frac{Z_0}{R_s} + 1 \gamma a + 0((\gamma a)^2) \right\}^{-1} \qquad \text{as } s \rightarrow 0 \tag{9.3}$$

In this form one can identify a time constant

$$t_h = \left[\frac{1}{3}\frac{Z_0}{R_s} + 1\right]\frac{a}{c} = t_{L/R} + t_t$$

$$t_{L/R} \equiv \frac{1}{3}\frac{\mu_0 a}{R_s} \equiv \text{"low frequency" L/R time constant}$$

$$t_t \equiv \frac{a}{c} \equiv \text{transit time for one radius}$$

(9.4)

Again a factor of $e^{-\gamma a}$ is included with $\tilde{f}_h(s)$ so as to make the time-domain form zero for negative time. In this case the low-frequency response of the normalized and delayed response function allows us to identify an L/R time constant appropriate to an inductive $\vec{H}$ or $\partial\vec{B}/\partial t$ sensor. Again this simple result only applies for electrically small sensors. At high frequencies the sensor is transit-time limited as reflected in the argument of the exponentials becoming comparable to unity.

Again taking our definition of upper frequency response as

$$\left| e^{-\frac{j\omega_c a}{c}} \frac{\tilde{f}_h(j\omega_c)}{\tilde{f}_{h_0}(j\omega_c)} \right| = \left| \frac{\tilde{f}_h(j\omega_c)}{\tilde{f}_{h_0}(j\omega_c)} \right| \equiv \frac{1}{\sqrt{2}}$$

(9.5)

at low frequencies we have found

$$\omega_c \simeq t_{L/R}^{-1} = \frac{3R_s}{\mu_0 a}$$

$$\frac{\omega_c a}{c} \simeq \left[\frac{ct_{L/R}}{a}\right]^{-1} = \frac{3R_s}{Z_0}$$

(9.6)

Figure 9.1 is a graph of $e^{-\frac{j\omega a}{c}}\tilde{f}_h(j\omega)/\tilde{f}_{h_0}(j\omega)$ as a function of the normalized frequency $\omega a/c$ with selected values of R_s/Z_0 as a parameter.

Using (9.5) to define ω_c then fig. 9.2 has $\omega_c a/c$ as a function of R_s/Z_0. The behavior of (9.6) is followed at low frequencies, but $\omega_c a/c$ tends to about 1.81 as $R_s/Z_0 \to \infty$.

Finally the figure of merit

$$\Lambda^{(h)} = \frac{\left[P^{(h)}_{ideal}(j\omega_c)\right]^{\frac{1}{2}}}{|\tilde{H}_{ref}(j\omega_c)|} \; Z_0^{-\frac{1}{2}} \; \frac{\omega_c}{c}$$

$$= \left[6\pi \; \frac{R_s}{Z_0}\right]^{\frac{1}{2}} \frac{\omega_c a}{c} \; |\tilde{f}_{h_0}(j\omega_c)|$$

$$= \left[\frac{2\pi}{3} \; \frac{Z_0}{R_s}\right]^{\frac{1}{2}} \left[\frac{\omega_c a}{c}\right]^2$$

is plotted as a function of R_s/Z_0 in fig. 9.3. As R_s/Z_0 is increased we find a maximum given by

$$\Lambda^{(h)}_{max} \simeq 1.9241$$

$$\frac{R_s}{Z_0} \simeq 1.54$$

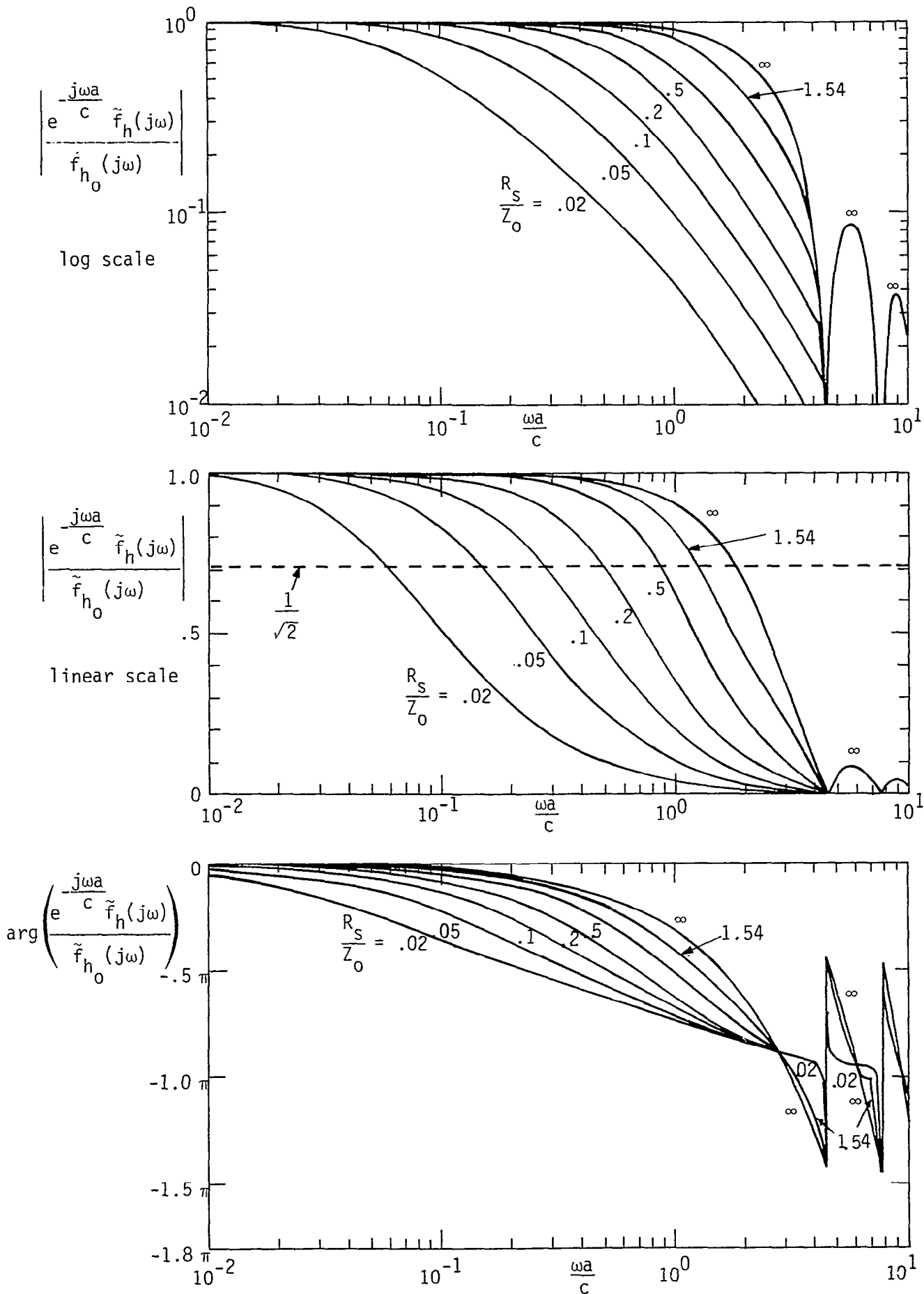$$\frac{\omega_c a}{c} \simeq 1.29$$

37

Figure 9.1. Magnetic-Dipole Response Versus Frequency
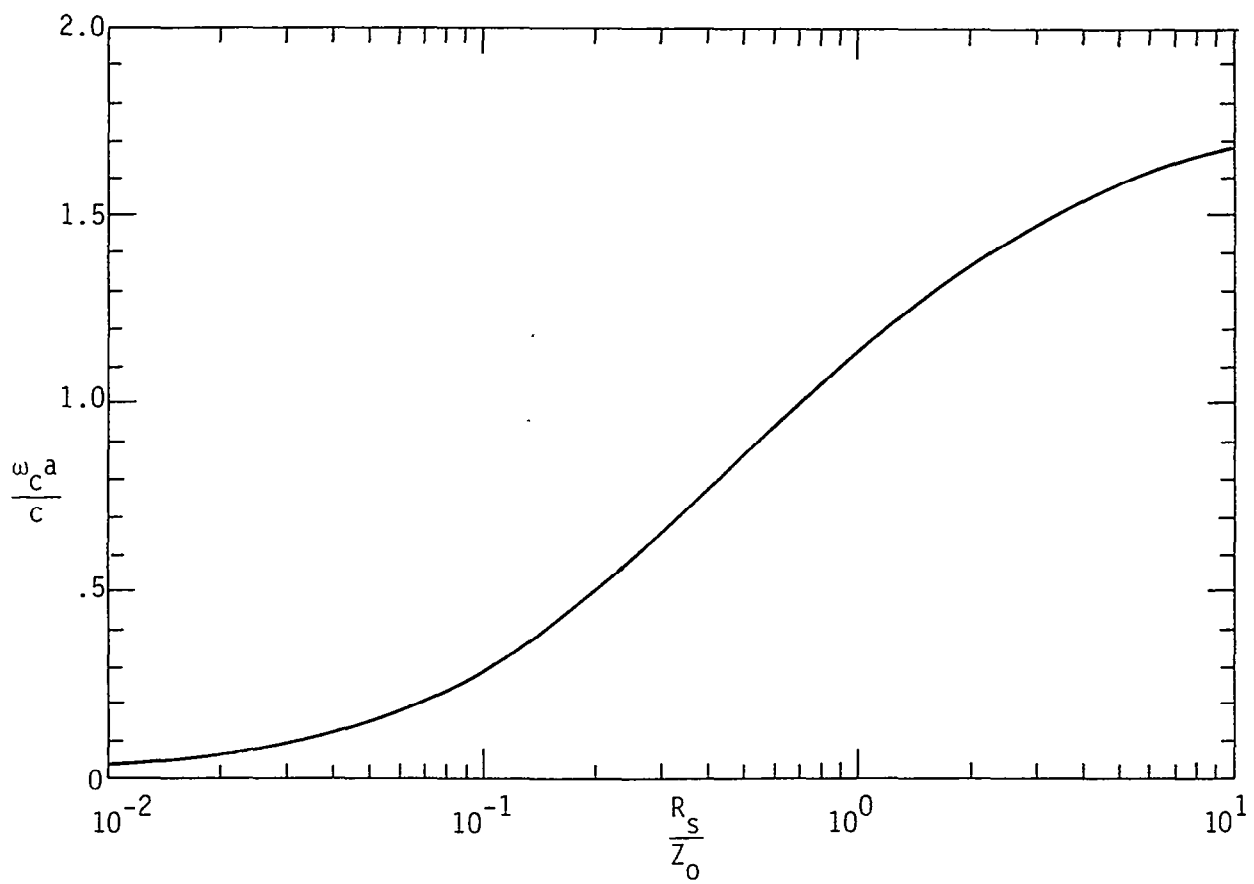
38

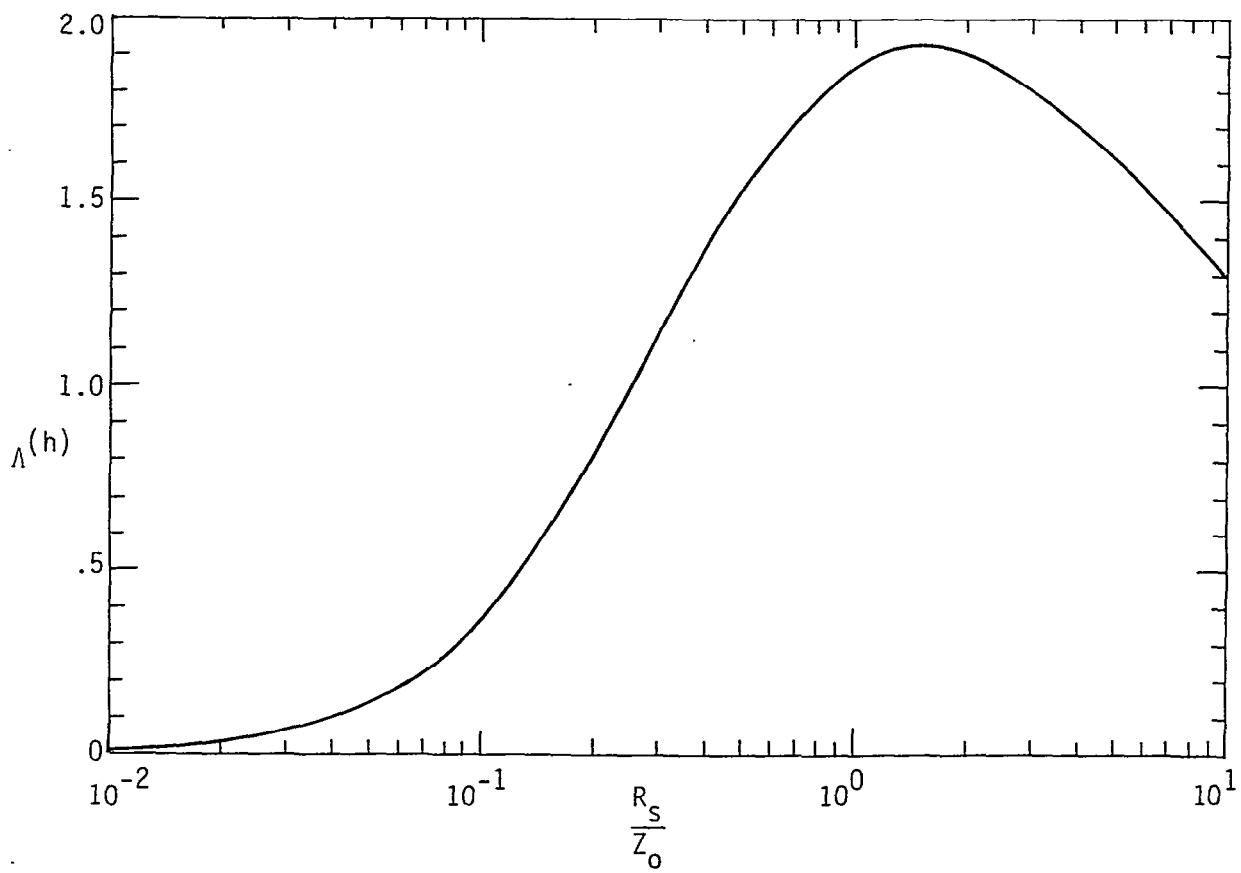Figure 9.2. Magnetic-Dipole Upper Frequency Response

Figure 9.3.   Magnetic-Dipole Figure of Merit

X. Application to Non-Ideal Sensors

Practical electromagnetic sensors are not accurately characterized as sheet impedance spheres. However, spherical modes can still be used to characterize the response.

Assume that some information (calculations or experimental data) exists concerning the response of a sensor (say voltage at defined terminals into a resistive load for an incident plane wave) of the form

$$\tilde{V}(\theta',\phi';s) = \sum_{n=1}^{\infty} \sum_{m=0}^{n} \sum_{p=e,0} \tilde{V}_{n,m,p}(s) Y_{n,m,p}(\theta',\phi') \tag{10.1}$$

This expresses the idea that for fixed s a function of (θ',ϕ') on the unit sphere can be expanded in terms of spherical harmonics which form a complete orthogonal set. Here θ' is taken as the angle of the field component of interest from the z axis. Note that the $n = 0$ term is omitted since the monopole term is absent in antenna response.

Let $\vec{1}_e$ or $\vec{1}_1$ indicate the direction of the incident electric or magnetic field, respectively, so that

$$\vec{1}_{\substack{e \\ h}} \cdot \vec{1}_z = \cos(\theta') \tag{10.2}$$

which is of the same form as the ideal angular behavior of the sensor response. The angle ϕ' is specified by the projection of $\vec{1}_{\substack{e \\ h}}$ on the x,y plane as

$$\vec{1}_{\substack{e \\ h}} \cdot \vec{1}_x = \sin(\theta')\cos(\phi')$$

$$\vec{1}_{\substack{e \\ h}} \cdot \vec{1}_y = \sin(\theta')\sin(\phi') \tag{10.3}$$

Taking $\vec{1}_2$ as

$$\vec{1}_2 = \pm\vec{1}_e \quad \text{or} \quad \vec{1}_2 = \pm\vec{1}_h \tag{10.4}$$

we can relate the (θ_1,ϕ_1) coordinates to the (θ',ϕ') coordinates as

$$\theta_1 = \begin{cases} \phi' + \frac{\pi}{2} & \text{for } 0 \leq \theta' \leq \frac{\pi}{2} \\ \pi \text{ or } 0 & \text{for } \theta' = \frac{\pi}{2} \\ \theta' - \frac{\pi}{2} & \text{for } \frac{\pi}{2} < \theta' \leq \pi \end{cases}$$

(10.5)

$$\phi_1 = \phi'$$

Strictly speaking one also needs to account for polarization. However, a plane wave propagating in the $\vec{1}_1$ direction can be considered as having a linear combination of waves characterized by $\vec{1}_2$ and $\vec{1}_3$ polarization given by (4.4). A particular choice of polarization is illustrated in (5.1). Let us choose the incident E field or H field to be polarized in the $\vec{1}_2$ direction, depending on whether we are considering respectively electric or magnetic sensors. Let the sensor axis, i.e., direction of its equivalent area, be oriented parallel to the z axis so that

$$\vec{A}_{e_{eq}} = A_{e_{eq}} \vec{1}_{e_{eq}} \quad , \quad A_{e_{eq}} > 0$$

$$\vec{1}_{e_{eq}} = \vec{1}_z$$

(10.6)

$$\vec{A}_{h_{eq}} = A_{h_{eq}} \vec{1}_{h_{eq}} \quad , \quad A_{h_{eq}} > 0$$

$$\vec{1}_{h_{eq}} = \vec{1}_z$$

In this convention θ' measures the angle of the field of interest (electric or magnetic) with respect to the z axis which is taken as the sensor axis. Now the $\vec{1}_3$ polarization is always orthogonal to the z axis, i.e.,

$$\vec{1}_3 \cdot \vec{1}_z = 0$$

(10.7)

Now if the sensor is properly symmetric with respect to the x,y plane, the sensor will not be sensitive to the electric or magnetic field component

parallel to $\vec{1}_3$; let us assume the presence of such symmetry so that we only need to consider the component parallel to $\vec{1}_2$.

Besides reflection symmetry with respect to the x,y plane [11] there are other symmetry considerations. The sensor can be in some sense symmetrically positioned or "centered" with respect to the z axis. In some cases (as with electric sensors) the sensor may be a body of revolution with respect to the z axis, such as the HSD (hollow spherical dipole) [4] or the ACD (asymptotic conical dipole) [3]. In other cases (as with magnetic sensors) the sensor may have one or more symmetry planes containing the z axis, such as the MGL (multi-gap loop) [2] which has 4 such symmetry planes spaced at angles of $\pi/4$ in its common realization.

Returning to (10.1) note that

$$Y_{1,0,e}(\theta',\phi') = P_1^{(0)}(\cos(\theta'))$$

$$= \cos(\theta') \tag{10.8}$$

This is precisely the term in (10.1) of interest, being the same as in (10.2). Furthermore, this term is orthogonal on the unit sphere to all the other scalar spherical harmonics in (10.1). Hence we can compute

$$\int_0^{2\pi}\int_0^{\pi} \tilde{V}(\theta',\phi';s)\cos(\theta')\sin(\theta')d\theta'd\phi'$$

$$= \tilde{V}_{1,0,e}(s) \int_0^{2\pi}\int_0^{\pi} \cos^2(\theta')\sin(\theta')d\theta'd\phi'$$

$$= V_{1,0,e}(s)\ 2\pi \int_0^{\pi} \cos^2(\theta')\sin(\theta')d\theta'$$

$$= -V_{1,0,e}(s)\ 2\pi \int_0^{\pi} \cos^2(\theta')d\,\cos(\theta')$$

$$= \frac{4\pi}{3}\ V_{1,0,e}(s) \tag{10.9}$$

giving

$$\tilde{g}(s) \equiv \tilde{V}_{1,0,e}(s) = \frac{3}{4\pi} \int_0^{2\pi} \int_0^{\pi} \tilde{V}(\theta',\phi';s)\cos(\theta')\sin(\theta')d\theta'd\phi' \qquad (10.10)$$

so that the dipole part of the response is $\tilde{g}(s)\cos(\theta')$. This can then be calculated from the measured response $\tilde{V}(\theta',\phi';s)$.

From the measured sensor response one can then calculate the electric- or magnetic-dipole part which can be normalized from

$$\tilde{g}_e(s) \sim \tilde{g}_{e_0}(s) = Z_c s\varepsilon_0 \tilde{E}_{ref}(s)A_{e_{eq}} \qquad \text{as } s \to 0$$

$$\qquad (10.11)$$

$$\tilde{g}_h(s) \sim \tilde{g}_{h_0}(s) = s\mu_0 \tilde{H}_{ref}(s)A_{h_{eq}} \qquad \text{as } s \to 0$$

giving

$$\tilde{G}_e(s) \equiv \frac{\tilde{g}_e(s)}{\tilde{g}_{e_0}(s)} = \frac{\tilde{g}_e(s)}{Z_c s\varepsilon_0 \tilde{E}_{ref}(s)A_{e_{eq}}} \to 1 \qquad \text{as } s \to 0$$

$$\qquad (10.12)$$

$$\tilde{G}_h(s) \equiv \frac{\tilde{g}_h(s)}{\tilde{g}_{e_0}(s)} = \frac{\tilde{g}_h(s)}{s\mu_0 \tilde{H}_{ref}(s)A_{e_{eq}}} \to 1 \qquad \text{as } s \to 0$$

as normalized dipole parts of the response.

We are now in a position to consider upper frequency response. Since $\tilde{V}(\theta',\phi';s)$ may have different frequency response functions for different (θ',ϕ') we need to choose which response functions to use. Our first choice is an appropriate average over (θ',ϕ'), in particular what we have defined as the dipole part. In normalized form we can define ω_c as the smallest ω_c for which

$$|\tilde{G}_e(j\omega_c)| = \frac{1}{\sqrt{2}}$$

$$\qquad (10.13)$$

$$|\tilde{G}_h(j\omega_c)| = \frac{1}{\sqrt{2}}$$

44

for electric- and magnetic-dipole sensors, respectively. Of course one should be concerned that $\tilde{G}_e$ or $\tilde{G}_h$ is not too dispersive so as to adversely affect the transient response; in such a case one may wish to construct $\tilde{G}_e(s)/s$ or $\tilde{G}_h(s)/s$ and inverse transform to obtain a step-function-like response from which an appropriate characteristic time for the rise can be defined (and which can be converted to an effective ω_c if desired).

Now using (10.13) to define ω_c may be limited to cases in which $\tilde{V}(\theta',\phi';s)$ does not deviate too much from $\tilde{g}(s)\cos(\theta')$ at least for frequencies up to ω_c. To treat the angular errors define

$$\alpha_{e \atop h}(\omega) = \frac{\| \tilde{V}(\theta',\phi';j\omega) - \tilde{g}_{e \atop h}(j\omega)\cos(\theta') \|}{\| \tilde{g}_{e \atop h}(j\omega) \|} \tag{10.14}$$

where the norm is taken over the range of (θ',ϕ') on the unit sphere. Norms can be defined in many ways [14]. A common norm is the infinity norm given by

$$\| \tilde{V}(\theta',\phi';j\omega) - \tilde{g}_{e \atop h}(j\omega)\cos(\theta') \|_\infty \equiv \max_{\theta',\phi'} \; | \tilde{V}(\theta',\phi';j\omega) - \tilde{g}_{e \atop h}(j\omega)\cos(\theta') |$$

$$\tag{10.15}$$

$$\| \tilde{g}_{e \atop h}(j\omega) \| \equiv | \tilde{g}_{e \atop h}(j\omega) |$$

In this form $\alpha_{e \atop h}^{(\infty)}(\omega)$ represents the maximum deviation from the "ideal" normalized to the magnitude of the "ideal" at its maximum, $\theta' = 0$. If $\alpha_{e \atop h}^{(\infty)}(\omega)$ for $\omega \le \omega_c$ is sufficiently small then (10.13) is adequate for defining bandwidth Conversely, if $\alpha_{e \atop h}^{(\infty)}(\omega)$ becomes larger than, say, $1/\sqrt{2}$ for $\omega \le \omega_c$ with ω_c from (10.13), then ω_c can be defined from (10.14) as the smallest ω_c for which

$$\alpha_{e \atop h}(\omega) = \alpha_0 \tag{10.16}$$

which is any convenient positive number which is not too large and in general is less than one.

There are various other norms such as the euclidean norm or 2 norm given by

$$\alpha_{\underset{h}{e}}^{(2)}(\omega) = \left\{ \frac{\displaystyle\int_0^{2\pi}\int_0^{\pi} |\tilde{V}(\theta',\phi';j\omega) - \tilde{g}_{\underset{h}{e}}(j\omega)\cos(\theta')|^2 \sin(\theta')d\theta'd\phi'}{4\pi|\tilde{g}_{\underset{h}{e}}(j\omega)|^2} \right\}^{\frac{1}{2}} \tag{10.17}$$

All of these norms can be approximately computed from measured (or calculated) response functions for the sensor.

XI.   Application to Magnetic Sensor Design

As mentioned before, the idealized spherical sensor can serve as a basis for approximate realization of a practical sensor. An example of a previously considered spherical-sensor design is the HSD (hollow spherical dipole) which has a perfectly conducting spherical shell loaded along an equatorial slot [4]. An efficient non-spherical magnetic-sensor design is the MGL (multi-gap loop) which is based on conducting cylindrical shell with its length approximately equal to its diameter and loaded at eight positions on the circular cylindrical shell [2]. It would be interesting to base a loop design on an approximately spherical shape.

In designing complex loop structures there are various techniques and constraints concerned with the use of transmission lines (impedances, transit times, and topologies) for the purpose of taking the signals from the load points or "gaps" to a common collection position [1]. For parallel combination of signals from different loops it is desirable to have the same voltages from each loop (except for perhaps single-ended/differential considerations). This implies that the loop areas be in the ratio of small integers so that the use of multiple (2, 3, etc.) or fractional (1/2, etc.) turns with these loops can give appropriate equivalent areas for each loop to match the outputs of the various loops.

As an example consider the design illustrated in fig. 11.1 for 3 loops labelled A, B, and C. These have radii and areas

$$\text{radius (A)} = \frac{a}{\sqrt{2}} \quad , \quad \text{area (A)} = \frac{\pi}{2} a^2$$

$$\text{radius (B)} = a \quad , \quad \text{area (B)} = \pi a^2 \tag{11.1}$$

$$\text{radius (C)} = \frac{a}{\sqrt{2}} \quad , \quad \text{area (C)} = \frac{\pi}{2} a^2$$

Centering the loop conductors for loops A and C on the defining sphere of radius a at angles of $\pi/4$ from the z axis makes the areas of loops A and C exactly half that of loop A. Then set the loop turns as (for example)
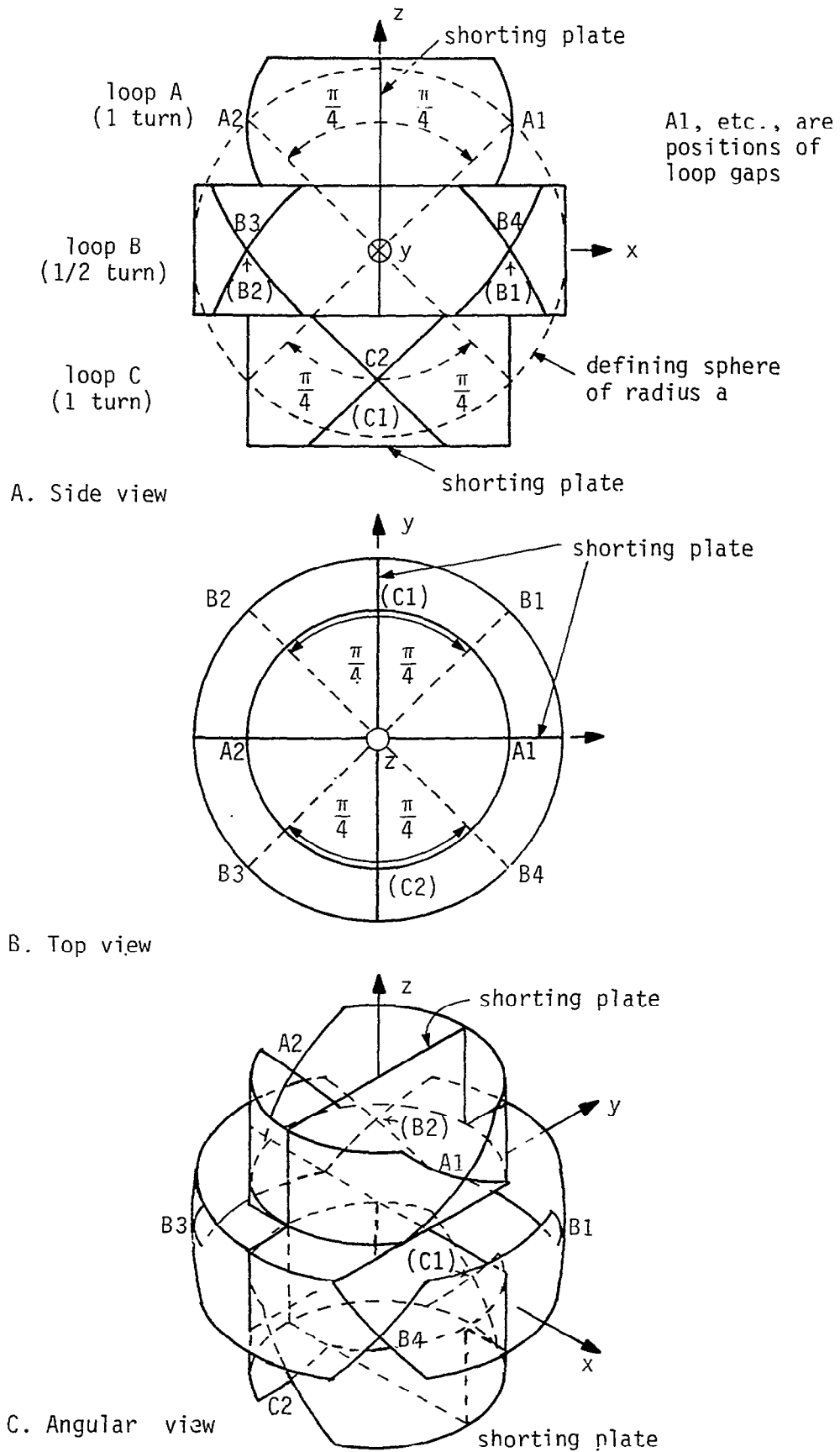
Figure 11.1. Three-Loop Spherical Magnetic-Field Sensor

48

$$\text{turns (A)} = 1 \quad , \quad A_{eq}(A) = \frac{\pi}{2} a^2$$

$$\text{turns (B)} = \frac{1}{2} \quad , \quad A_{eq}(\ddot{B}) = \frac{\pi}{2} a^2 \tag{11.2}$$

$$\text{turns (C)} = 1 \quad , \quad A_{eq}(C) = \frac{\pi}{2} a^2$$

This gives equal equivalent areas so that the loop outputs may be connected in parallel without introducing an ambiguity in the equivalent area of the sensor. Note that .the loop is made of wide strips instead of thin wires to reduce the inductance.

Our example shows loop B with 4 load points or "gaps" labelled B1 through B4. Each gap is made of a 200 Ω conical transmission line (as in the typical MGL) driving a 200 Ω transmission line leading along the loop conductors and shorting plates to the summing position in the center presenting two 400 Ω differential signals there to be added in parallel. Loops A and C each have two such gaps, each driving 200 Ω transmission lines to the summing position where each presents a 400 Ω differential signal there to be added in parallel to each other and to the B signals.. The resulting four 400 Ω differential signals in parallel give

$$Z_C = 100 \ \Omega \quad \text{(differential)} \tag{11.3}$$

which is quite convenient. Note that in fig. 11.1 load points in parentheses are in the "back," hidden from view by the sensor conductors.

This sensor design attempts to approximate a sphere of sheet resistance R_s by these 8 symmetrically positioned signal sampling positions, each of 200 Ω, on the surface of a sphere of radius a. One can roughly estimate R_s from say loop B by taking it to encompass an angular width of $\pi/4$ or width $a\pi/4$ with a circumference $2\pi a$ giving

$$R_s \simeq 4(200 \ \Omega) \frac{\pi a}{4} \frac{1}{2\pi a} = 100 \ \Omega \tag{11.4}$$

Other sheet resistances can also be approximated by changing the number of gaps and/or gap impedances.

One can also envision other similar magnetic sensor designs involving say 4 loops. The 2 loop case is approximated by the typical MGL design already.

XII. Conclusion

This note has explored the optimization of time-derivative electromagnetic-field sensors. Using the concept of figure of merit an idealized spherical type of sensor is used to investigate the maximization of this parameter. Using a definition of bandwidth that the normalized response is reduced to $1/\sqrt{2}$ of its low-frequency value gives figures of merit approaching 2 for the idealized spherical sensors, both electric and magnetic, in this note. For comparison one may look at some recently obtained measurements of the response of the MGL and ACD sensors [10]. These have figures of merit scattered in the same general magnitude as the maximum figures of merit (almost 2) for the idealized sensors here. Note that the angular errors discussed in section 10, when applied to the MGL and ACD, did not become serious until significantly above the upper frequency response.

The idealized spherical sensors discussed here do not exhaust all the possibilities for consideration of maximum possible figure of merit. Other possible types of spherical sensors include ones with other radial distributions of impedance loading (instead of a shell or delta function with respect to r). Furthermore, other kinds of impedance loading functions besides a purely resistive one could be considered. Some kind of RLC network (distributed) could be used for $\tilde{Z}_s(s)$ with one of the resistances representing the effective impedance of the output transmission lines; the remaining elements might be used to optimize the sensor performance near the upper frequency response. Much is still needed to understand what is practically attainable in optimized upper frequency response.

References

1. C. E. Baum, A Technique for the Distribution of Signal Inputs to Loops, Sensor and Simulation Note 23, July 1966.

2. C. E. Baum, The Multi-Gap Cylindrical Loop in Nonconducting Media, Sensor and Simulation Note 41, May 1967.

3. C. E. Baum, An Equivalent-Charge Method for Defining Geometries of Dipole Antennas, Sensor and Simulation Note 72, January 1969.

4. C. E. Baum, The Single-Gap Hollow Spherical Dipole in Nonconducting Media, Sensor and Simulation Note 91, July 1969.

5. C. E. Baum, A Technique for Simulating the System Generated Electro-magnetic Pulse Resulting from an Exoatmospheric Nuclear Weapons Radiation Environment, Sensor and Simulation Note 156, September 1972.

6. C. E. Baum, A Figure of Merit for Transit-Time Limited Time-Derivative Electromagnetic Field Sensors, Sensor and Simulation Note 212, December 1975.

7. C. E. Baum, E. L. Breen, J. C. Giles, J. P. O'Neill, and G. D. Sower, Sensors for Electromagnetic Pulse Measurements Both Inside and Away From Nuclear Source Regions, Sensor and Simulation Note 239, January 1978, IEEE Transactions on Antennas and Propagation, January 1978, pp 22-35, and IEEE Transactions on Electromagnetic Compatibility, February 1978, pp. 22-35.

8. C. E. Baum, Sensors for Measurement of Intense Electromagnetic Pulses, Sensor and Simulation Note 271, June 1982, and Proceedings of 3rd IEEE International Pulsed Power Conference, Albuquerque, June 1981.

9. C. E. Baum, E. L. Breen, F. L. Pitts, G. D. Sower, and M. E. Thomas, The Measurement of Lightning Environmental Parameters Related to Interaction with Electronic Systems, Sensor and Simulation Note 274, May 1982, and IEEE Transactions on Electromagnetic Compatibility, May 1982, pp. 123-137.

10. V. V. Liepa and T.B.A. Senior, Measured Characteristics of MGL and ACD Sensors, Sensor and Simulation Note 276, September 1982.

11. C. E. Baum, Interaction of Electromagnetic Fields with an Object Which Has an Electromagnetic Symmetry Plane, Interaction Note 63, March 1971.

12. C. E. Baum, On the Singularity Expansion Method for the Solution of Electromagnetic Interaction Problems, Interaction Note 88, December 1971.

13. R. L. Gardner and C. E. Baum, Expansion of a Scalar, Vector, or Dyadic Function in Terms of the Spherical Vector Wave Functions, Mathematics Note 36, May 1974.

14. C. E. Baum, Norms and Eigenvector Norms, Mathematics Note 63, November 1979.

15. P. M. Morse and H. Feshbach, Methods of Theoretical Physics, McGraw Hill, 1953.